Structural and immunomodulatory properties of bioactive polysaccharide from solid-state fermented brown rice with *Antrodia cinnamomea* mycelia

Potchanee Kaewkumsan[1†], Mohsen Gavahian[1†], Wei-Ting Tseng[2†], Jia-Hsin Guo[1*]

[1]Department of Food Science, College of Agriculture, National Pingtung University of Science and Technology, 1, Shuefu Road, Neipu, Pingtung, 912301, Taiwan, ROC; [2]Lytone Enterprise Inc., Xizhi, New Taipei City, 22180, Taiwan, ROC

[†]These authors contributed equally as the co-first author to this work.

[*]**Corresponding Author:** Jia-Hsin Guo, Department of Food Science, College of Agriculture, National Pingtung University of Science and Technology, 1, Shuefu Road, Neipu, Pingtung, 912301, Taiwan, ROC. Email: jhguo@mail.npust.edu.tw

Academic Editor: Walid Elefalleh, PhD, Department of Life Sciences, Al Imam Mohamed Ibn Saud Islamic University (IMSIU), 11623 Riyadh, Saudi Arabia, and Higher Institute of Applied Sciences and Technology of Gabes (ISSATGb), Tunisia

Received: 16 April 2025; Accepted: 26 May 2025; Published: 1 July 2025

RESEARCH ARTICLE

Abstract

Natural polysaccharides derived from edible fungi efficiently modulate the immune system typically without adverse effects. In this work, a strain isolated from wild fruiting bodies of *Antrodia cinnamomea* (AC), identified via *18S ribosomal RNA* gene sequencing, was used in solid-state fermentation of brown rice at 27°C for 3, 6, and 10 months to develop polysaccharide. Bioactive polysaccharide was isolated by ultrasonic-assisted enzymatic extraction and gel permeation chromatography prior to structural analysis and immunomodulatory studies in rat peripheral blood mononuclear cells (PBMCs) and RAW 264.7 mouse macrophages. AC polysaccharide fraction I (ACP-I) increased by 20.8-fold (47.08 μg/mL) at 6 months of fermentation. Unlike typical fungal heteroglucans, ACP-I was identified as a unique heterogalactan (29.2 kDa), predominantly featuring terminal fucose residues. The immunomodulatory studies in lipopolysaccharide-stimulated macrophages demonstrated that ACP-I suppressed nitric oxide (NO) production through downregulating inducible NO synthase level and nuclear factor kappa B activation, which consequently suppressed pro-inflammatory cytokine expression, including interleukin 8, interferon beta-1, and CC chemokine RANTES, without affecting macrophage inflammatory protein-2 levels. Additionally, ACP-I promoted a 2.2-fold increase in PBMC proliferation, compared to concanavalin A, indicating dual immunomodulatory activity, which highlighted its potential as a nutraceutical and functional food ingredient for food and pharmaceutical applications.

Keywords: food nutrition improvement; functional food; immunomodulator; manufacturing innovation; solid-state fermentation; ultrasound

Introduction

Rice is a global dietary staple for billions of people. Whole grain rice, or brown rice (BR), is widely recognized for its health benefits because of its high dietary fiber content and bioactive compounds. Regular consumption of whole grains, including BR, has been linked to a reduced risk of several diet-related non-communicable diseases (NCDs),

such as diabetes, cardiovascular diseases, and certain types of cancers (Ikeda *et al.*, 2025). However, BR is not widely consumed due to its coarse texture and low palatability. To address this issue, various processing methods, including innovative non-thermal and fermentation techniques, have been explored to enhance its taste and consumer acceptance.

Antrodia cinnamomea (syn. *Antrodia camphorata*), known in Chinese as "Niu-Chang-Chih" or "Ruby of the forest," is an extremely rare edible and medicinal mushroom native to forested regions of Taiwan (Zhang *et al.*, 2019). AC belongs to the phylum *Basidiomycetes* and the family *Polyporaceae*. For long, it has been used to treat liver diseases and promote recovery of the liver from food, alcohol, and drug poisoning (Ganesan *et al.*, 2019). Polysaccharides serve as the primary active constituent of AC (Xia *et al.*, 2022). Recently, edible fungal polysaccharides have gained significant attention in the field of functional foods and nutraceuticals because of their diverse health-promoting properties (Punthi *et al.*, 2023). Aqueous extraction has been widely used to obtain water-soluble polysaccharides from various edible fungi that exert potent immune functions (Pérez-Bassart *et al.*, 2023; Punthi *et al.*, 2025). Fungal bioactive polysaccharides are studied extensively for *β*-D-glucans because of their therapeutic effects on inflammatory diseases and cancers (Zhang *et al.*, 2019). *β*-D-glucans exist abundantly in the cell walls of fungi and cereals as homopolysaccharides, which are made up of repeating units of D-glucose (Vetvicka *et al.*, 2021). To date, not only *β*-D-glucans but heteropolysaccharides with more complex and diverse structures are considered one of fungi's most crucial bioactive components. AC polysaccharides have shown the potential in immune responses, such as regulating macrophage activation and inflammatory response to infectious hepatitis B virus and *Schistosoma mansoni* (Wang *et al.*, 2019) and suppressing progression of tumors by maintaining or restoring immune homeostasis (Hou *et al.*, 2020). Notably, the immune response can act as a double-edged sword, protecting and potentially harming the host. Thus, the use of polysaccharides as natural immunomodulators with immune-stimulating and anti-inflammatory functions is a mild yet effective therapeutic approach with fewer adverse effects.

Previous studies have shown significant impact of polysaccharide biomodification by fungal fermentation on their physicochemical and biological properties (Chakraborty *et al.*, 2021). In addition, the structural diversity of monosaccharide compositions and glycosidic linkages has been reported to contribute to diverse biological activities (Shen *et al.*, 2024). It has been known that the biological functions of fungal polysaccharides are diverse and depend on fungal strains and polysaccharides' chemical structure. Yet, insufficient preparative methods and structural characterization remain a gap between structural variability and bioactivity. Therefore, for industrial-scale production, quality control of fungal bioactive polysaccharides is essential for fermentation, extraction, and purification processes, ensuring consistency based on their specific functional properties. Further research is needed to elucidate the detailed relationship between polysaccharide structure and function to support their continued development and application as functional foods and therapeutic agents in health supplements and clinical treatments.

Solid-state fermentation (SSF) is used for traditional Asian food production. Over the last two decades, SSF has emerged as a versatile technology for developing industrial bioprocesses because of its cost-effectiveness, environment-friendliness, high productivity, and decreased risk of contamination (Mattedi *et al.*, 2023). SSF is a traditional cultivation technique for microbial metabolite production. The fermentation process utilizes a solid matrix without free-flowing water, which is appropriate for filamentous fungi. Solid substrate serves as a nutrient source and a supporting matter for microbial growth without additional free water. The fermentation container can be simply constructed as a metal and lid or non-airflow box to promote the uniform growth of mycelia or microorganisms (Manan and Webb, 2017).

In addition to SSF, submerged fermentation (SmF) is another bioprocess for microbial metabolites. SmF is developed for industrial scale-up continuous usage, online monitoring, and automatic control systems. However, SSF significantly impacts productivity and product characteristics more than SmF. SSF is observed to support microbial growth in an environment that closely mimics their natural habitat, which consequently enhances biomass and metabolite production. Therefore, filamentous fungi can produce plenty of metabolites under SSF conditions. For example, biomass and pigments of five filamentous fungi (*Talaromyces verruculosus*, *Fusarium solani*, *Penicillium multicolour*, *P. canescens*, and *P. herquie*) remarkedly increased to more than 10 times using SSF higher than SmF (Molelekoa *et al.*, 2021). SSF enhanced cellulase production by the fungus *Trichoderma reesei* with less environmental impact on the production system than SmF. In addition, SSF elevated the hydrolytic performance and initial reaction rate of biomass hydrolyzing enzymes, such as β-glucosidase and xylanase, derived from *Penicillium janthinellum* National Culture Collection of Industrial Microorganisms (NCIM) 1366 culture (Sankar *et al.*, 2023). Current studies on SSF have increased attention to the functional and nutritional value of plant-based agro-industrial residuals. It is considered an alternative approach to improve physicochemical properties and bioavailability of primary cereal staple foods, such as rice,

maize, and wheat (Lim *et al.*, 2024; Omarini *et al.*, 2019). SSF enhances BR's nutrient bioavailability, breaks down anti-nutritional factors like phytic acid, and increases total phenolic content. Furthermore, SSF of rice bran reduces lipid content (48.5 to 27.8%), while increasing total carbohydrates (36.6 to 50.2%), proteins (7.4 to 12.8%), and ash (7.6 to 11.5%). Accumulating studies have shown that SSF is well adapted for fungi and can improve the biological activity of natural compounds.

The present study aimed to isolate and characterize a novel bioactive polysaccharide (ACP-I) from AC-fermented BR using SSF, focusing on its unique immunomodulatory properties, including enhancing innate immunity and suppressing inflammation. The immunomodulatory activity of crude and purified polysaccharides was evaluated using an *ex vivo* model of rat peripheral blood mononuclear cells (PBMCs), and the bioactive polysaccharide was chosen for further analysis in RAW 264.7 mouse macrophages. The chemical composition and preliminary structure of bioactive polysaccharide were characterized by high-performance gel permeation chromatography (HPGPC), gas chromatography (GC), gas chromatography–mass spectrometry (GC-MS), Fourier-transform infrared spectroscopy (FT-IR), and proton nuclear magnetic resonance (^{1}H NMR) spectroscopy.

Materials and Methods

Materials and reagents

Malt extract agar (MEA) and malt extract broth (MEB) were purchased from BD Difco (MD, USA). BR (*Oryza sativa* L. var. *japonica*) was purchased from Sie Chern Rice Factory (Taitung, Taiwan). α-Amylase and amyloglucosidase were of food grade (Trump Chemicals, Taipei, Taiwan). Sugar standards (L-(+)-rhamnose monohydrate, D-(+)-maltose monohydrate, D-(+)-raffinose pentahydrate, D-glucose, D-galactose, D-mannose, D-xylose, L-fucose, and L-arabinose) and myo-inositol were purchased from Sigma-Aldrich (MO, USA), and the Pullulan calibration kit were purchased from Showa Denko America Inc. (NY, USA). Trifluoroacetic acid (TFA), sodium borohydride, methyl iodide, 1-methylimidazole, sodium borodeuteride, acetic anhydride, ammonium hydroxide, dimethyl sulfoxide (DMSO), Triton X-100, and concanavalin A (ConA) were acquired from Sigma-Aldrich. Sodium hydroxide (NaOH), sodium chloride (NaCl), acetic acid, and dichloromethane were purchased from Merck KGaA (Darmstadt, Germany). Diethyl pyrocarbonate (DEPC)-treated water, AlamarBlue® dye (resazurin), RPMI-1640, fetal bovine serum (FBS), penicillin–streptomycin (100 U/mL penicillin and 100 μg/mL streptomycin), and Dulbecco's phosphate buffered saline (PBS) were purchased from Invitrogen (CA, USA). Ethylene diamine tetraacetic acid (EDTA), Ficoll-Paque Premium, and agarose were purchased from Promega (WI, USA), GE Healthcare (Buckinghamshire, UK), and Amresco (OH, USA), respectively. All chemicals and reagents were of analytical grade.

Isolation and identification of filamentous fungus

Wild fruiting bodies of AC were collected from mountain valleys of Yuli Township, Hualien, Taiwan (latitude: 23°21'00.0"N; longitude: 121°21'00.0"E). Each sample of the fruiting bodies was incubated separately on MEA under optimum conditions at 15°C for 2–3 days in the dark. The newly grown mycelia were transferred to fresh MEA and cultivated for an additional 7 days. We observed the morphologies and culture characteristics of fully grown mycelia under a microscope and stored agar plates at 4°C for subsequent subculturing. The isolated fungal strain, termed NPU-50, was selected for further study based on its relatively fastest growth, deep red color, and intense aroma. The newly grown mycelia after 7-day cultivation were frozen in liquid nitrogen and crunched into powder using a sterilized mortar and pestle. According to the supplier's instructions, the genomic deoxyribonucleic acid (DNA) from approximately 100 mg of the powder was extracted using a genomic DNA purification kit (Fermentas, Ontario, Canada).

DNA fragments were amplified using the GeneAmp PCR System (TP600, Takara Bio Inc., Shiga, Japan). We used the *18S ribosomal RNA* (*18S rRNA*) gene sequences of published universal fungi primers NS3 and NS6 (Wu *et al.*, 2015) to identify the fugal strains as shown in Table 1. The Polymerase chain reaction (PCR) reaction was performed with 50 μL of extracted DNA solution, 2 μL of each primer, and 50 μL of PCR Master Mix containing 2.5 units of Taq DNA polymerase, reaction buffer, 4-mM $MgCl_2$, and 0.4-mM of each deoxynucleotide triphosphate (dNTP).

The PCR cycles were set as follows: each cycle consisted of an initial denaturation time of 2 min at 98°C, followed by 35 cycles of amplification comprising a denaturation step for 45 s at 95°C, annealing at 52°C for 45 s, and extension at 72°C for 2 min. Reactions were completed with elongation for 10 min at 72°C, followed by cooling at 4°C. The PCR-amplified DNA fragments were sequenced by Tri-I Biotech Inc. (Taipei, Taiwan). The sequenced NPU-50 genome was 100% identical to the *18S rRNA* gene of AC strain CMY01 (AY336795.1) using the Basic Local Alignment Search Tool (BLAST) and National Center for Biotechnology Information (NCBI) reference sequences. NPU-50 strain was deposited at the Bioresource Collection and Research Center (BCRC), Food Industry

Table 1. Primers used in the present study.

Gene	Primer	Sequence	Length (bp)
NS3	Forward	5'-GCAAGTCTGGTGCCAGCAGCC-3'	21
NS6	Reverse	5'-GCATCACAGACCTGTTATTGCCTC-3'	24
IFN-β1	Forward	5'-GCTCCAAGAAAGGACGAACA-3'	20
	Reverse	5'-GGATGGCAAAGGCAGTGTAA-3'	20
MIP-2	Forward	5'-CACTCTCAAGGGCGGTCAAA-3'	20
	Reverse	5'-AGGCACATCAGGTACGATCCA-3'	21
RANTES	Forward	5'-GAAGGAACCGCCCAAGTGTGT-3'	21
	Reverse	5'-GAGCAAGCGATGACAGGGAA-3'	20
β-actin	Forward	5'-TGGTGGGAATGGGTCAGAA-3'	19
	Reverse	5'-TCTCCATGTCGTCCCAGTTG-3'	20
GAPDH	Forward	5'-CCACAGTCCATGCCATCACT-3'	20
	Reverse	5'-GGATGCAGGGATGATGTTCTG-3'	21

Notes: NS3 and NS6: universal fungi primers; *IFN-β1*: interferon beta-1; *MIP-2*: macrophage inflammatory protein-2; *RANTES*: regulated on activation, normal T-cell expressed and secreted, or CC chemokine ligand 5; *β-actin*: cytoskeleton housekeeping gene; *GAPDH*: glyceraldehyde-3-phosphate dehydrogenase.

Research and Development Institute, Hsinchu, Taiwan (BCRC930127. 29).

Solid-state fermentation

Solid-state fermentation was performed according to our previously reported method (Taiwan patent No. TWI395813B; Guo and Tseng, 2015). Briefly, BR was inoculated with AC in a round stainless steel box (16 × 8 cm) with a lid and locking clips. BR (200 g) was soaked in 190-mL distilled water overnight and then autoclaved at 121°C for 30 min. The soaking water was replaced with 190-mL MEB. The BR was inoculated with 7-day-old filamentous fungus and incubated at 27°C in a dark room for 3, 6, and 10 months to achieve optimal mycelial growth of AC. The fermented BR with fully grown AC mycelia was lyophilized and kept in a humidity control chamber at a relative humidity of 50% for extracting and isolating polysaccharides as illustrated in Figure 1.

Extraction and isolation of polysaccharide fractions

Polysaccharides were extracted from the AC-fermented BR using an ultrasonic-assisted enzymatic extraction method. A 20-g sample was mixed with 300 mL of deionized water in a 500-mL flask. The mixture was then sonicated in an ultrasonic bath at a frequency of 40 kHz and a maximum power of 800 W at a pre-heated temperature of 30–80°C for 30 min. Sequential enzymatic hydrolysis was performed by adding 5.0 g/L of α-amylase for 15 min, followed by amyloglucosidase for 50 min. A cold water bath was used to prevent overheating of the mixture. The crude extract was centrifuged (13,400×g) at 4°C for 20 min to remove insoluble substances. Then, polysaccharides were precipitated with four volumes of 95% (v/v) ethanol at 4°C for 24 h. The precipitate was washed twice and vacuum-dried with 70% (v/v) ethanol. An aqueous polysaccharide solution was prepared and filtered through a 0.45-μm nylon membrane. We used a PD-10 column (Sephadex G-25, GE Healthcare) to remove small molecule impurities and obtain crude polysaccharides. HPGPC was performed using a Sephacryl S-300 HR column and ultraviolet/visible (UV/Vis) detector. The polysaccharide fractions were isolated with a mobile phase, 0.05-M NaCl, at a 0.5-mL/min flow rate. Each fraction (8 mL) was collected by a Frac-920 fraction collector (GE Healthcare). Total sugars were measured at 490 nm by the phenol-sulfuric acid method (Yue *et al.*, 2022). The modified Lowry method determined the protein content using the BCA protein assay kit (Pierce Biotechnology, IL, USA) and bovine serum albumin as a standard. The pooled fractions were applied individually to a PD-10 column to replace NaCl solution with deionized water before being lyophilized and stored at -20°C. The fraction powder's moisture content was determined using a moisture analyzer (MB45; OHAUS, NJ, USA).

Cell proliferation assay of PBMCs

Twenty healthy male CD® IGS rats (BioLASCO, Taoyuan, Taiwan) were acclimatized to the Laboratory Animal Facility for 2 weeks under controlled conditions (22 ± 1°C, 65 ± 10% humidity, and a 12-h light–dark cycle) with food and water provided *ad libitum*. All procedures were conducted according to animal care and

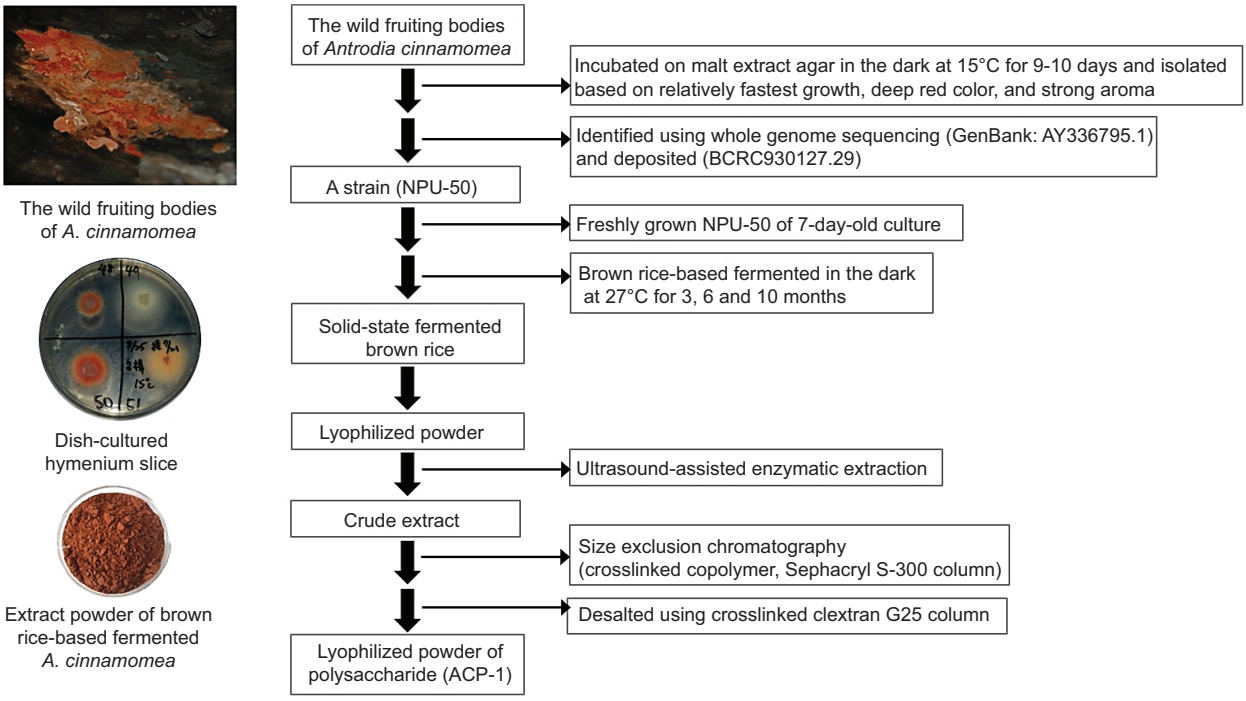

Figure 1. The preparation process of bioactive polysaccharide ACP-I from solid-state fermented brown rice using *A. cinnamomea*.

handling protocols approved by the Institutional Animal Care and Use Committee of National Pingtung University of Science and Technology (NPUST-IACUC-0951221). The animals (aged 7–8 weeks, weighing 250–290 g) were anesthetized with Avertin (Sigma-Aldrich), and blood samples (about 20 mL per animal) were collected via cardiac puncture under deep anesthesia. All rat carcasses were covered and kept at -20°C for subsequent collection by an animal carcass processing facility.

Peripheral blood mononuclear cells were isolated according to previously described methods (Režić-Mužinić *et al.*, 2018; Yue *et al.*, 2010). Briefly, rat blood was collected in a vacutainer EDTA tube (16 × 100 mm; Becton Dickinson, NJ, USA) and centrifuged at 300×g for 15 min at 20°C. The buffy coat layer was transferred into a sterile 15-mL centrifuge tube and diluted with sterile PBS at a ratio of 1:1. An equal volume of Ficoll–Paque (density 1.077 g/mL, 3 mL) was gently added to the blood-saline solution using following method. The mixture was centrifuged at 700×g for 15 min at 20°C with a brake off to obtain a thin white middle layer of PBMCs. The collected PBMCs were washed with at least three volumes of PBS (10 mL) and centrifuged at 300×g for 15 min at 20°C. The supernatant was discarded, and the pellet was resuspended in RPMI-1640 medium at a cell density of 2×10^6 cells/mL.

The cell suspension was seeded in 96-well plates for an *ex vivo* proliferation assay. Each cell suspension (50 µL) was mixed with 50 µL of various polysaccharide fractions separately to a final concentration of 150 µg/mL with or without ConA (10 µg/mL). Lipopolysaccharide (LPS) was also added to the cells at a final concentration of 1 µg/mL as a positive control to observe endotoxin response. The plate was incubated in a humidified 5% CO_2 incubator at 37°C for 72 h. An AlamarBlue® dye (10 µL) was then added to each well, and the plate was further incubated for 4 h. Absorbance was measured at 570 nm using a microplate reader (PowerWave XS, BioTek, VT, USA) with a reference wavelength of 600 nm.

Chemical and structural analysis of bioactive polysacchride fraction

Molecular weight determination

The molecular weight (MW) of bioactive polysaccharide fraction (ACP-I) was analyzed by HPGPC using an analytical high-performance liquid chromatography (HPLC) equipped with a TSKgel G3000PW$_{XL}$ column (7.8 mm × 30.0 cm; Tosoh, Tokyo, Japan) and a refractive index (RI) detector (L-2490; Hitachi, Tokyo, Japan) (Dong *et al.*, 2019). ACP-I solution (10 mg/mL) was prepared in a mobile phase (0.05-M NaCl solution) and filtered through a 0.45-µm nylon membrane. An aliquot (20 µL) of the solution was analyzed at 35 ± 1°C with a 0.6 mL/min flow rate. The average MW was calculated using a calibration curve of sugar and pullulan standards (180,182, 360, 594, 6,100, 22,000, and 110,000 Da).

Monosaccharide composition analysis

Monosaccharide composition was analyzed using GC (HP 5890A; Hewlett Packard, CA, USA) equipped with an HP-5 capillary column (0.25 mm × 30 m, 0.15 μm) and a flame-ionization detector (FID). ACP-I (5 mg) was hydrolyzed in a capped tube with 2-M TFA (0.3 mL) at 121°C for 90 min (Barnes *et al.*, 2021). After hydrolysis, TFA residue was repeatedly co-evaporated to dryness with methanol under a nitrogen stream. Myo-inositol (1 mg) was added as an internal standard. The hydrolysate was reduced and acetylated by the previous method with some modifications (Chen *et al.*, 2017a). Briefly, the hydrolysate was reduced by sodium borohydride (2 mL) for 90 min at room temperature and then neutralized with glacial acetic acid (0.1 mL). The alditols were acetylated with acetic anhydride (2 mL) using 1-methylimidazole (0.2 mL) as a catalyst for 10 min at room temperature. The excess acid was neutralized with deionized water (5 mL). The alditol acetates were extracted with dichloromethane (1 mL), washed with deionized water (10 mL) for three times, and evaporated under a nitrogen stream. The resulting alditol acetates were dissolved in dichloromethane, and an aliquot (2 μL) was analyzed by GC using ultra-pure nitrogen as a carrier gas at a flow rate of 1.1 mL/min. The column oven was maintained at 220°C (Dong *et al.*, 2019). Injector and detector were set at 250°C and 270°C, respectively.

Glycosidic linkage analysis

The glycosidic linkage of ACP-I was analyzed by methylation (Chen *et al.*, 2017b), followed by hydrolysis, reduction, and acetylation (Barnes *et al.*, 2021; Black *et al.*, 2019; Higashi and Toida, 2017) according to previously described methods with some modification. ACP-I (5 mg) was suspended in anhydrous DMSO (0.5 mL) and sonicated to a complete solution. The sample was methylated twice with NaOH solution (0.5 mL, 1-M NaOH in DMSO) and methyl iodine (0.4 mL) in a capped tube. After 30 min, deionized water (2 mL) was added. Permethylated products were extracted with dichloromethane (1 mL) and dried under a nitrogen stream. The sample was then hydrolyzed with 2-M TFA (0.3 mL) at 121°C for 90 min. TFA was removed by repeated evaporation with methanol under a nitrogen stream. The sample was reduced with sodium borodeuteride (1 mL, 20 mg/mL [w/v] in 2-M aqueous NH_3) for 1 h at room temperature. Glacial acetic acid (0.1 mL) was added to stop the reaction. The partially methylated alditol acetates (PMAAs) were obtained by acetylation and extraction with dichloromethane, as described in Section 2.6.2. The resulting PMAAs were analyzed by GC-MS (Agilent 5973; MSD, CA, USA) using an HP-5 capillary column (0.25 mm × 30 m, 0.15 μm). The column temperature was programmed from 50°C to 130°C (40°C/min), held for 2 min, and then increased to 230°C (4°C/min), held for 9 min.

Functional group analysis

ACP-I (2 mg) mixed with potassium bromide (100 mg) was dried at 110°C for 20 min and pressed into a pellet by a hydraulic pressing machine (400 kg/cm^2). FT-IR spectra were recorded from 4,000 cm^{-1} to 400 cm^{-1} at room temperature (25°C) using an FT-IR spectrometer (IR 300; Thermo, Osterode, Germany).

Configuration analysis

^{1}H NMR spectroscopy was used to verify α/β-configured glycosidic bonds in ACP-I based on vicinal coupling constants (Nepravishta *et al.*, 2021). ^{1}H NMR spectra were recorded at 27°C (Bhanja and Rout, 2017) on a Varian 400 MHz NMR system (AS400; Agilent, CA, USA) using a 5-mm broadband probe (Barnes *et al.*, 2021). ACP-I (5 mg) was exchanged with deuterium oxide or heavy water (D_2O; 0.5 mL, 99.9% D, Sigma-Aldrich). The chemical shifts were expressed in parts per million (ppm).

Immunomodulatory activity of bioactive polysaccharide fraction

Cell culture and treatment

RAW 264.7 mouse macrophage cells (Manassas, VA, USA) were cultured in RPMI-1640, supplemented with 10% FBS and 1% penicillin–streptomycin under 5% CO_2 at 37°C. Cells were seeded in six-well plates (5 × 10^5 cells/well) overnight prior to treatment with ACP-I (100–150 μg/mL) for 30 min–24 h. The medium was replaced with fresh medium containing either LPS (1 μg/mL) as a positive control or PBS as an untreated control, and the cells were further incubated for 30 min–8 h. The treated cells were collected for cytoplasmic and nuclear protein extraction.

Measurement of nitric oxide (NO) and inducible nitric oxide synthase (iNOS)

RAW 264.7 cells were seeded in 96-well plates (1 × 10^4 cells/well) overnight prior to treatment with ACP-I (100–150 μg/mL) in the presence or absence of LPS (0.1 μg/mL) for 6, 12, and 24 h. NO production in culture supernatant was measured as nitrite (), a stable metabolic NO, using Griess reagent (A: 1% [w/v] sulfanilamide, and B: 0.1% [w/v] N-(1-naphthyl)ethylenediamine in 2.5% [v/v] phosphoric acid), and $NaNO_2$ as a standard (Vargas-Maya *et al.*, 2021). The supernatant (100 μL) was mixed with the Griess reagents A (50 μL) and B (50 μL) and incubated for 10 min at room temperature in the dark. The colored azo dye product was measured at 540 nm using a microplate reader (SPECTROSTAR Nano; BMG Labtech, Germany). Whole-cell proteins were extracted after 24-h treatment using the method described in Section 2.7.3. According to the supplier's instructions, iNOS levels were measured by Enzyme-linked-immunosorbent serologic assay (ELISA) using a mouse iNOS ELISA kit (Invitrogen).

Cytoplasmic and nuclear protein extraction and western blot analysis

To extract whole-cell proteins, we washed the cells for two times with ice-cold PBS prior to lysis on ice for 5 min with M-PER mammalian protein extraction reagent (Thermo Scientific, IL, USA) containing extra protease inhibitors: 1-mM phenylmethanesulfonyl fluoride (PMSF), 2-μg/mL pepstatin A, and 10-μg/mL leupeptin (MP Biomedicals, OH, USA). After a freeze-thaw cycle (30 min at -80°C), the cell lysate was centrifuged (18,000×g) for 10 min at 4°C to collect supernatant for the Western blot analysis of IκB-α protein.

The cytoplasmic and nuclear proteins were extracted using a previously described method with some modifications (Martynova *et al.*, 2021). Cells were washed and harvested into 1.5-mL tubes at a density of 2×10^6 cells/tube. The cell suspension was centrifuged (3,000×g) for 5 min at 4°C. Cell pellet was lysed on ice for 10 min in a 200-μL lysis buffer A (10-mM Tris-HCl, pH 7.4, 10-mM NaCl, 3-mM $MgCl_2$, and 0.5% NP-40, in DEPC-treated water) containing protease inhibitor cocktail: 1-mM PMSF, 1-μg/mL pepstatin A, 1-μg/mL leupeptin, 1-mM sodium fluoride (NaF), and 1-μg/m laprotinin (MP Biomedicals). The lysate was centrifuged to obtain supernatant containing cytoplasmic proteins. The nuclear pellet was washed with lysis buffer A (200 μL) without NP-40 and protease inhibitors, followed by centrifugation to discard the supernatant. Nuclear proteins were extracted using lysis buffer B (10-mM Tris-HCl, pH 7.4, 400-mM NaCl, 1-mM EDTA, and 1-mM DL-dithiothreitol (DTT), in DEPC-treated water) with protease inhibitor cocktail. Then, nuclear proteins were lysed in buffer B (70 μL) with vigorous shaking for 30 min at 4°C. The supernatant was obtained by centrifuge (12,000×g) for 10 min at 4°C. The protein content was quantified using a Bradford protein assay kit (Bio-Rad, CA, USA). Nuclear factor kappa B (NF-κB) p65 protein was blotted using β-actin and H3 as loading controls. Protein samples were mixed with a loading buffer containing 5% β-mercaptoethanol and boiled for 5 min. Samples (40 μg) were loaded on 20% sodium dodecyl sulfate polyacrylamide gel and then transferred to a 0.45-μm nitrocellulose membrane (Bio-Rad). The membrane was incubated overnight with a specified primary antibody at 4°C and the secondary antibody for 1 h at room temperature. Antigen–antibody complexes were detected by enhanced chemiluminescence reagent (Bio-Rad) on Flour Chem-FC2 Imaging System (Alpha Innotech, CA, USA).

NF-κB-dependent luciferase activity assay

RAW 264.7 cells were transfected with a luciferase reporter plasmid according to the manufacturer's directions. We used a pGL-3 backbone and β-galactosidase control vector (Promega), constructed with an interleukin 8 (IL-8) promoter in DH-5α *E. coli* strain. Briefly, cells were seeded in 24-well plates (1×10^5 cells/well) and serum-starved for 24 h. The medium was replaced with Opti-MEM (Invitrogen) for 2 h before co-transfected with IL-8 promoter (0.4 μg) and luciferase reporter plasmid (0.1 μg) for 6 h. Then, cells were incubated with RPMI-1640 medium containing ACP-I (100 μg/mL) for 12 h, followed by LPS challenge (1 μg/mL) for 8 h. The luciferase activity was measured with the Dual-Luciferase® Reporter Assay System (Promega).

RNA analysis

Total RNA was isolated from RAW 264.7 cells using TRI Reagent® (Ambion, TX, USA), and complementary DNA (cDNA) was synthesized using a reverse transcriptase kit (Invitrogen) as per manufacturer's instructions. Quantitative reverse transcription polymerase chain reaction (qRT-PCR) was conducted using SYBR® Green master mix (Bio-Rad) under standard conditions (95°C for 5 min, 1 cycle; 95°C for 15 s and 60°C for 1 min, 40 cycles) on a CFX connect real-time system (Bio-Rad). Mouse primers for qRT-PCR, including IFN-β1, MIP-2, RANTES, β-actin, and GAPDH, were shown in Table 1. All reactions were run in triplicate, and the expression levels of the target genes were normalized with a housekeeping gene, *β-actin* or *GAPDH*, using the 2-ΔΔCT method.

Statistical analysis

Data were expressed as mean values ± standard deviation (SD) from three independent experiments. Each experiment was performed in triplicate. Statistical analysis was carried out using One-Way Analysis of Variance (ANOVA), followed by Tukey's Honestly Significant Difference (HSD) test. The statistical assumptions of normality and homogeneity were assessed using the Shapiro–Wilk test and Levene's test, respectively. The Mann–Whitney U test was employed for nonparametric data. Statistical significance was defined as $P < 0.05$.

Results and Discussions

Solid-state fermentation of brown rice

The fruiting bodies of AC were collected and isolated to almost 100 mycelial strains with different morphologies. An intense red colony with relatively fastest growth and strong aroma was selected and identified using the universal fungal primers NS3 and NS6 to amplify a successful PCR product of the isolated genomes (approximately 740 bp) of AC strain NPU-50. BLAST homology search revealed that the unedited sequences were 100% identical to the *18S rRNA* gene sequences of AC strain CMY01 (AY336795.1). The NPU-50 strain was deposited (BCRC930127, Taiwan) and used in the SSF of BR.

The NPU-50 strain of AC exhibited extensive white mycelium formation on BR during the initial 3 months of SSF. This changed to a brownish red with a strong camphor aroma after fermentation for 6 months. At the end of the 10-month fermentation, the fermented BR formed a sponge-like structure with a strong aroma. Figures 2A and 2B (overlaid) show initial polysaccharide production patterns and after 3, 6, and 10 months of fermentation. The BR polysaccharide constituent, peak 3 at the retention time of 13.68 min decreased continuously during fermentation. The fermented product, peak 2 (12.11 min) was observed slightly whereas peak 1 (10.8 min) increased gradually to the maximum for up to 6 months of fermentation. The results indicated that peak 1 was mainly produced by AC during SSF, while peak 2 might be the fragments resulting from fungal degradation of complex polysaccharides in BR.

Extraction, isolation, and molecular weight distribution of polysaccharides

Crude polysaccharide with the extraction rate of 6.86 ± 0.06% (dry basis) was obtained from BR with fully grown AC mycelia at 10-month fermentation, comparable to hot water extraction (yield 6.65%) from lyophilized powder of AC (Liu *et al.*, 2017). The moisture content of polysaccharide powder was 10.03 ± 0.81%. The protein contents were low (<0.07 ± 0.03 mg/g crude polysaccharides). As illustrated in Figure 2C, polysaccharide fraction I (4.82%), II (0.07%), III (1.84%), and trace components (0.13%) were isolated by HPGPC using cross-linked dextrans (Sephacryl S-300 HR and Sephadex G-25). Figure 2D shows the size distribution of polysaccharide fractions, namely ACP-I, ACP-II, and ACP-III. Each fraction was further purified to homogeneity by removing soluble components with MW < 5 kDa using a Sephadex G-25 column. The low MW components (8.1 and 1.7 kDa) were removed during purification. The average MW of polysaccharides was determined using HPGPC-RI with TSKgel G3000PW$_{XL}$ column, pre-calibrated with standard sugars and pullulans (MW range: 0.18–110 kDa). According to calibration curve (log MW = 9.060–0.425 t, R^2 = 0.994), the average MW of ACP-I was calculated as 29.2 kDa. The elution profile of ACP-I in Figure 2E shows a single and symmetrical narrow peak, indicating a high purity and homogeneity of fraction.

Immunostimulating activity of polysaccharide fractions on PBMCs

The polysaccharide fractions were tested in an *ex vivo* model of rat PBMCs to examine their effect on PBMC proliferation, compared with crude polysaccharide extract and control groups. According to the Alamar Blue

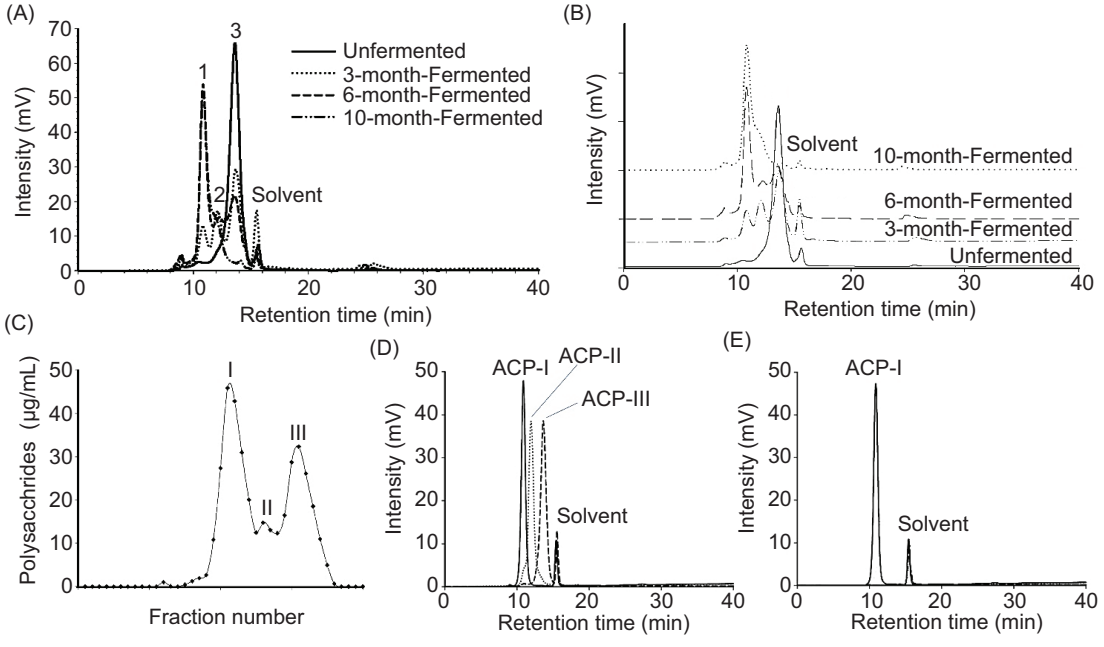

Figure 2. Isolation of polysaccharides from solid-state fermentation of brown rice using *A. cinnamomea* for 0 (unfermented), 3, 6, and 10 months of fermentation period. (A and B) HPLC-RI chromatograms of crude polysaccharide products. (C) Polysaccharide fractions, ACP-I, ACP-II, and ACP-III were isolated from the 10-month fermented brown rice by HPGPC. (D) Overlay of HPGPC-RI chromatograms of ACP-I, ACP-II, and ACP-III after isolation and purification. (E) HPGPC-RI chromatogram of ACP-I showed a single and symmetrical peak, indicating that the purified polysaccharide was homogeneous.

assay, there was no adverse effect on cell cytotoxicity after exposure to polysaccharide fractions, Con A, and LPS at test levels for 72 h (Supplementary Table S1). As shown in Figure 3, ACP-I significantly enhanced ConA-induced proliferation of PBMCs after treatment ($P < 0.05$). The co-incubation with ACP-I (150 µg/mL) and ConA (10 µg/mL) synergistically increased cell proliferation by 2.2-fold, compared to ConA alone. A significant but lower proliferation was observed if PBMCs were exposed to ACP-II (1.3-fold) and ACP-III (1.8-fold). Compared with PBS (control group without treatment), exposure to ACP-I in the presence of ConA increased proliferation by 6.1-fold, followed by ACP-III (4.8-fold) and ACP-II (3.0-fold). The results implied that ACP-I exhibited the highest immunostimulatory activity on PBMCs among other polysaccharide fractions and crude extract.

Peripheral blood mononuclear cells are widely used as an *in vitro* model to investigate the effect of food-bioactive compounds on various immune cells (Kleiveland, 2015). PBMCs are easily obtainable blood cell fractions and comprise a heterogeneous population of immune cells, including lymphocytes (T, B, and NK cells), granulocytes, and monocytes. These blood cells are key components of the immune system that defend against and adapt to invaders. Herein, rat PBMCs were used. The PBMC populations commonly vary across individuals, but typically, rat lymphocytes are about 79.1–82.0%, followed by 12.9–14.3% granulocytes, and 5.2–7.1% monocytes (Peakman *et al.*, 1993). PBMC proliferation is considered an indicator of cellular and humoral immune responses, primarily driven by T and B cells (Marshall *et al.*, 2018).

For screening immune-enhancing polysaccharide fractions, a mitogen-induced proliferation assay of PBMCs was performed to evaluate nonspecific immune response to invading pathogens. ConA and LPS were mitogens that stimulate lymphocytes nonspecifically. ConA is a plant lectin and a well-known T-cell mitogen. LPS is an endotoxin present in the cell walls of Gram-negative bacteria that are well recognized by monocytes and murine B cells (Jeon *et al.*, 2021). An LPS dose of 0.1–10 µg/mL was reported to induce murine B-cell proliferation within 48 h (Chaiwut and Kasinrerk, 2022).

In the present study, PBMC proliferation significantly increased after 72 h of LPS stimulation (1 µg/mL). In the presence of LPS, ACP-I could elicit PBMC proliferation comparable to ConA alone ($P \geq 0.05$). Notably, proliferation increased by three-fold after treatment with ACP-I and ConA, compared to that of LPS. Given that, rather than B lymphocytes, LPS probably induced innate (or natural) responses by monocytes (monocytes, macrophages, and dendritic cells) or granulocytes (neutrophils) (Tucureanu *et al.*, 2018). However, their populations (8–21% of PBMCs) were much lower than lymphocytes, and yet, LPS alone might be less sufficient to activate B cells, which require a typical pattern of adaptive (or acquired) immunity (Glaros *et al.*, 2021). It is still unclear whether LPS specifically activated monocytes and pro-inflammatory responses in PBMCs.

According to the results, ACP-I had the maximum potential to enhance immune responses among polysaccharide fractions. ACP-I significantly boosted the proliferative response of PBMCs to ConA but not LPS. Unlike ACP-I, BR polysaccharide (ACP-III) did not affect LPS-induced PBMC proliferation. In contrast, the fragments (ACP-II) increased the LPS-induced cytotoxic response of PBMCs, compared to the control groups ($P < 0.05$). Therefore, ACP-I was considered a bioactive polysaccharide and was chosen for further analysis.

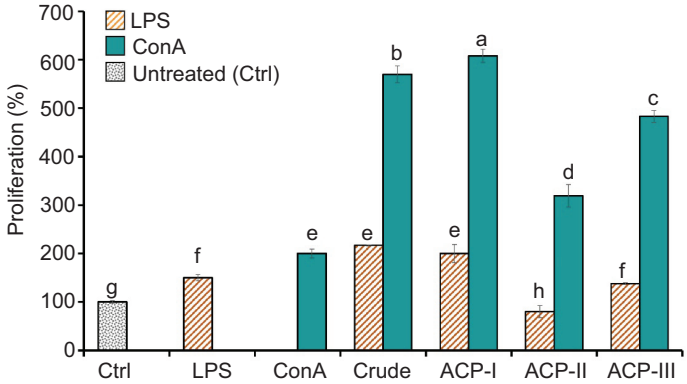

Figure 3. Effect of crude extract and polysaccharide fractions, ACP-I, ACP-II, and ACP-III, isolated from solid-state fermented brown rice using *A. cinnamomea*, on the proliferation of rat PBMCs after treatment (150 µg/mL) in the presence of ConA (10 µg/mL) or LPS (1 µg/mL) for 72 h, compared with the control groups without treatment (Ctrl) and treated with ConA or LPS. Different letters show statistically significant differences ($P < 0.05$).

Monosaccharide composition and preliminary structural analysis of ACP-I

The monosaccharide composition of the bioactive polysaccharide fraction ACP-I was determined by hydrolysis, reduction, and methylation, followed by GC-FID analysis. The relative number of monosaccharides indicated that ACP-I consisted of galactose (43.75%), fucose (34.09%), glucose (14.20%), mannose (3.98%), and arabinose (3.98%) in a respective ratio of 11.0:8.6:3.8:1.0:1.0. The major monosaccharides of ACP-I were galactose, fucose, and glucose, accounting for 92.05% of all monosaccharide composition.

Glycosidic linkages of PMAAs from ACP-I were identified using GC-MS. The results revealed that ACP-I had a complex structure with seven types of glycosidic linkages, as shown in Table 2. ACP-I comprised five different monosaccharides through methylation alditol acetates and their parent sugars as measured by GC-FID. The chemical structure of ACP-I had a neutral sugar backbone or side chains for 58.52%, including galactose (68.92%), glucose (24.28%), and traces of arabinose (6.80%) in a ratio of 10.1:3.6:1.0. The galactose residuals were measured as →3,4)-Gal-(1→ and →6)-Gal-(1→ in a ratio of 10.7:1.0 with a total proportion of 40.33% in ACP-I. The proportion of galactose, glucose, and arabinose residuals was in accordance with the ratio of monosaccharide composition. It is noteworthy that →3,4)-Gal-(1→ residuals were the most linkage types in the main chain of ACP-I. While the →2,4,6)-Ara-(1→ and →6)-Gal-(1→ residuals were found in the lowest proportion of 3.98% and 3.44%, respectively, among three monosaccharide residuals in the main chain. The proportion of terminal residues was high (41.48%), mainly comprising fucose (82.18%), with a small amount of mannose (9.60%) and galactose (8.22%). Together with monosaccharides, the result suggested that ACP-I might constitute (1→3)- and (1→4)-linked galactan as well as a possible (1→6)-linked galactan, with branches possibly substituted at O-2, O-3, and O-6 of the 2,4-linked glucose, 2,4,6-linked arabinose, 3,4-linked galactose, and 1,6-linked galactose.

The FT-IR spectrum of ACP-I was scanned from 4,000 cm^{-1} to 400 cm^{-1} to obtain the basic information of functional groups (Figure 4A). The 3,490 cm^{-1} and 2,923 cm^{-1} peaks indicated the absorption of OH and CH bonds, involving the stretching and bending vibrations of CH, CH_2, or CH_3 (Xia *et al.*, 2022). Peaks at 1,723 cm^{-1} and 1,650 cm^{-1} were primarily due to the stretching vibration of C=O of ester carbonyl and carboxylate groups (Bai *et al.*, 2020). Weak peaks at 1,542–1,400 cm^{-1} were assigned to C–H deformation and vibrations (Xia *et al.*, 2022). The absence of peaks around 1,422 cm^{-1}, or 1,018–1,000 cm^{-1} as galacturonic acid (Chylińska *et al.*, 2016), indicated a small amount or lack of uronic acid after reduction. The fingerprint region of polysaccharides at 1,200–800 cm^{-1} was dominated by ring vibrations overlapping with stretching vibration of C–OH side groups and C–O–C glycosidic bond on pyran rings (Chylińska *et al.*, 2016). Absorption near 1,081 cm^{-1} was mainly due to C–O–C stretching in the pyran structure (Dong *et al.*, 2019). The characteristic band at 1,000–800 cm^{-1} indicated the presence of glycosidic linkages (Chylińska *et al.*, 2016). Peaks at 912 cm^{-1} and 873 cm^{-1} could be related to C–H bending vibration on β-pyran ring (Chylińska *et al.*, 2016). The peak at 810 cm^{-1} suggested the presence of α-glycosidic bonds. The spectrum indicated that the monosaccharide constituents of ACP-I existed in the cyclic pyranose form linked with α- and β-glycosidic linkages.

The ^1H NMR spectrum was further used to identify the α/β configuration of glycosidic linkages in ACP-I. The configuration of monosaccharide constituents was observed in D_2O at 27°C using ^1H NMR spectroscopy to monitor ^1H proton spectrum. The chemical shifts of significant signals were assigned regarding vicinal coupling constants of specific sugar residuals, as illustrated in Table

Table 2. GC-MS results of methylation analysis of polysaccharide fraction ACP-I, isolated from solid-state fermented brown rice using *A. cinnamomea*.

Peak No.	Methylated sugar	T*R* (min)	Molar ratio (%)	Fragmentation pattern (m/z)	Glycosidic linkage[a]
1	2,3,4-Me_3-Fuc	13.91	34.09	43, 72, 89, 101, 118, 131, 162, 174, 191, 446	T-Fuc-(1→
2	2,3,4,6-Me_4-Man	19.69	3.98	43, 71, 87, 102, 118, 129, 145, 161, 205, 446	T-Man-(1→
3	2,3,4,6-Me_4-Gal	20.21	3.41	43, 71, 88, 102, 112, 118, 130, 174, 190, 205, 234, 446	T-Gal-(1→
4	2,3,4-Me_3-Gal	22.71	3.44	43, 71, 87, 102, 118, 129, 147, 162, 189, 233, 446	→6)-Gal-(1→
5	2,6-Me_2-Gal	23.52	36.89	43, 71, 87, 99, 102, 118, 129, 142, 162, 173, 189, 233, 446	→3,4)-Gal-(1→
6	3,6-Me_2-Glc	24.31	14.21	43, 71, 87, 118, 129, 147, 159, 189, 204, 233, 281, 446	→2,4)-Glc-(1→
7	3-Me-Ara	25.62	3.98	43, 71, 87, 99, 118, 129, 143, 160, 189, 233, 243, 446	→2,4,6)-Ara-(1→

Notes: T_R: retention time; molar ratio: relative molar ratio; [a]T: terminal alditol acetate residues.

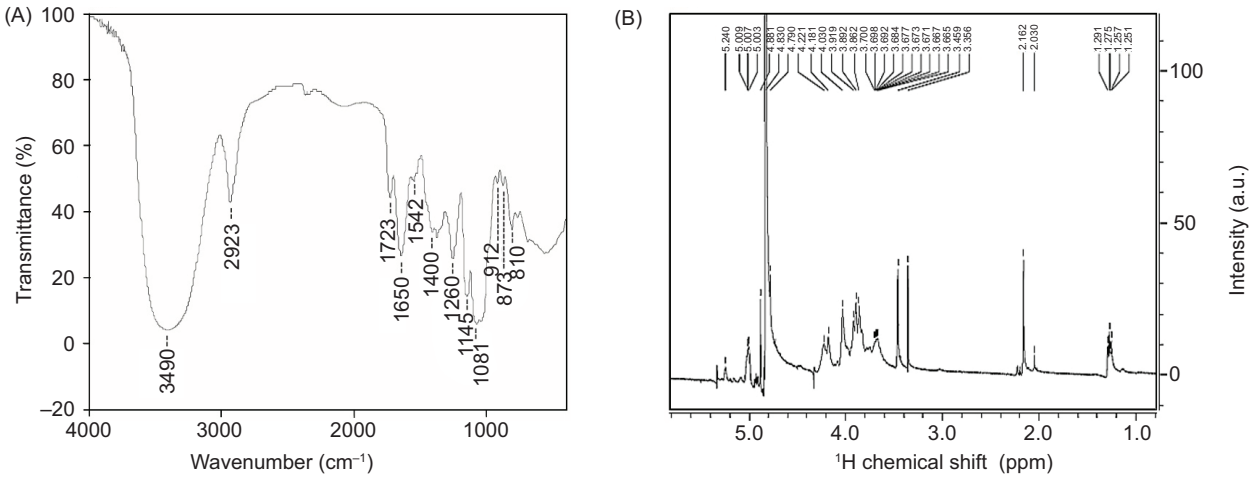

Figure 4. (A) FT-IR and (B) ^{1}H NMR spectra of polysaccharide fraction ACP-I, isolated from solid-state fermented brown rice using *A. cinnamomea*.

Table 3. Assignments of chemical shifts of polysaccharide fraction ACP-I, isolated from solid-state fermented brown rice using *A. cinnamomea* in the ^{1}H NMR spectrum.

Sugar residues	Chemical shifts, δ (ppm)						
	H-1	H-2	H-3	H-4	H-5	H-6	H-7
α-D-Man-(1→	4.88	3.98	3.83	3.70	3.70	3.78	3.89
α-D-Gal-(1→	5.24	3.84	3.90	4.02	4.34	3.69	3.71
β-D-Gal-(1→	4.79	3.52	3.67	3.92	3.71	3.78	3.75
α-L-Fuc-(1→	5.01	3.69	3.90	3.79	4.10-4.90[a]	–	–

Note: [a]Conformational change.

3. The ^{1}H NMR spectrum of ACP-I appeared in the region ranging from chemical shift (δ) 1.25 to δ 5.24 ppm (Figure 4B). However, only well-resolved signals of the anomeric region at δ 5.6–4.4 ppm were used to identify the configuration of monosaccharide units. The results demonstrated that four anomeric proton signals were observed at δ 5.24, δ 5.01, δ 4.88, and δ 4.79 ppm, which were assigned to α-D-galactopyranose (α-D-galactose), 6-deoxy-α-L-galactopyranose (α-L-fucose), α-D-mannopyranose (α-D-mannose), and α-D-galactopyranose (α-D-galactose), respectively. The signal peaks were within the range of 5.6–4.4 ppm, at which δ 5.6–4.9 ppm indicates α-anomers and δ 4.9–4.3 ppm indicates β-anomers (Speciale *et al.*, 2022). According to FT-IR spectrum (Figure 4A), the existence of both α- and β-glycosidic configurations was proved by ^{1}H NMR signals.

One-dimensional (1D) ^{1}H NMR spectrum of polysaccharides contains some well-resolved signals arising due to anomeric (δ 5.6–4.4 ppm) and aliphatic (δ 2.0–1.0 ppm) protons (Speciale *et al.*, 2022). For ACP-I, the signals of acetyl (δ 2.16–2.05 ppm) and methyl (δ 1.29–1.25 ppm) groups were relevant to deoxy sugar composition. A previous report also considered the methyl groups at δ 1.3–1.1 ppm as 6-deoxy-L-galactopyranose (L-fucose) and 6-deoxy-L-mannopyranose (L-rhamnose) (Speciale *et al.*, 2022). However, because of the perennial problem of limited chemical shift dispersion of nanometric protons, the ^{1}H NMR spectrum is far less sufficient to define the chain conformation of ACP-I, other than cyclic structures (D or L) and linkage pattern (α or β) of monosaccharide constituents.

Four different configurations of three main sugars, such as D-mannose, D-galactose, and L-fucose, were characterized, excluding glucose and arabinose, which were identified by GC-MS. This might be due to the low abundance of glucose (14.21%) and arabinose (3.98%) in ACP-I, which probably resulted in overlapped or masked signals. Even though MS is inherently more sensitive with lower detection limits than NMR, several advantages of NMR as a nondestructive, reproducible, and high-throughput method have made it particularly useful in food and metabonomic studies (Emwas *et al.*, 2019). The 1D ^{1}H NMR technique uses an optimized probe for ^{1}H detection, rather than other nuclei, such as ^{13}C and ^{15}N, thus providing informative anomeric proton signals for polysaccharide analysis (Speciale *et al.*, 2022).

Furthermore, a crowned part of carbinolic region (δ 4.4–3.0 ppm) is considered the fingerprint of polysaccharides that requires a combined use of 2D NMR (Speciale *et al.*, 2022). To date, the structural elucidation of polysaccharides and their substituents is developed by combining ^{1}H NMR with ultra high-resolution NMR, such as 1D fluorine-edited selective TOCSY acquisition (FESTA), 2D correlation spectroscopy (COSY), 2D nuclear Overhauser effect spectroscopy (NOESY), heteronuclear single quantum coherence (HSQC), and heteronuclear multiple bond coherence spectroscopy (HMBC) (Poškaitė *et al.*, 2023). Besides, an alternative strategy to improve ^{1}H dispersion may involve using chemical shifts of -OH groups as a starting point for structural assignment, combined with 2D NMR for resolution enhancement (Brown *et al.*, 2018). In this strategy, the OH resonances of sugar were rarely seen when its OH protons were exchanged with D_2O at room temperature, as a standard practice used in this study. An alternative solvent, such as dimethyl sulfoxide-d6 (DMSO-d6), would be used. Otherwise, OH resonances would be recorded in supercooled H_2O and D_2O, especially for bioactive polysaccharides whose structure–function relationship should be characterized under physiologically relevant conditions. Although NMR offers many advantages, a few limitations must be resolved regarding cost-efficient experiments and the combined use of supplemental techniques, such as GC and GC-MS (Eltemur *et al.*, 2023). These analytical techniques, eventually, are useful tools to identify known and unknown bioactive polysaccharides and other natural products.

In vitro immunomodulatory activity of ACP-I

Effect of ACP-I on NO and iNOS production in LPS-stimulated macrophages

Among the immune cells, macrophages play critical roles in inflammatory response by releasing mediators, such as reactive oxygen species (ROS), NO, cytokines, and chemokines (Bagaev *et al.*, 2019). Activated macrophages produce NO via iNOS enzyme as a toxic defense molecule against infectious organisms (Palmieri *et al.*, 2020). RAW 264.7 murine macrophage cell line is helpful in studying the molecular mechanisms of macrophages in immune regulation by recognizing pathogen-related molecular patterns (PAMPs) by toll-like receptors (TLRs).

In this study, RAW 264.7 macrophages were incubated with ACP-I (100–150 μg/mL) in the presence or absence of LPS (0.1 μg/mL) for 24 h. Production of NO was monitored at 6, 12, and 24 h of incubation using Griess reagent, and the level of iNOS was measured by ELISA at 24 h of incubation. As shown in Figure 5A, LPS induced NO production in RAW 264.7 cells ($P < 0.05$), but not ACP-I ($P \geq 0.05$). Interestingly, ACP-I could modulate NO production in LPS-stimulated RAW 264.7 cells after incubation for 12–24 h. This result was in accordance with the level of iNOS produced by RAW 264.7 cells during 24 h of incubation (Figure 5B). Compared with the untreated control, ACP-I at 100 μg/mL concentration did not affect iNOS level in RAW 264.7 cells ($P \geq 0.05$). Meanwhile, the iNOS level decreased by increasing the concentration of ACP-I (150 μg/mL; $P < 0.05$). The results indicated that ACP-I moderated NO production in LPS-stimulated RAW 264.7 cells by regulating iNOS expression in a concentration-dependent manner, likely through the suppression of NF-κB activation, which, in turn, downregulated the expression of pro-inflammatory cytokines, such as IL-8, IFN-β1, and RANTES.

Effect of ACP-I on NF-κB activation in LPS-stimulated macrophages

The innate immune response to pathogens and dangerous signals is initiated and guided by macrophages (Marshall *et al.*, 2018). LPS is a classical and potent agonist of TLR 4 in macrophages that triggers an acute inflammatory response via NF-κB activation. NF-κB is activated by the removal (phosphorylation and degradation) of inhibitory protein IκBα from NF-κB subunits, primarily p65 and p50, which then translocate into the nucleus and promote transactivation of target genes to produce pro-inflammatory cytokines (Bagaev *et al.*, 2019). In this study, nuclear translocation of p65 was monitored in LPS-stimulated RAW 264.7 macrophages to investigate the anti-inflammatory activity of ACP-I. Western blot analysis results revealed that ACP-I (100 μg/mL) suppressed LPS-induced NF-κB activation in RAW 264.7 cells by downregulating the degradation of IκBα and consequent nuclear translocation of p65. As illustrated in Figure 6, in resting cells (untreated control), p65 was localized in the cytoplasm (Figure 6A) but not in the nucleus (Figure 6B). In contrast to LPS-stimulated RAW 264.7 cells, the nuclear p65 increased significantly ($P < 0.05$). LPS could trigger the translocation of p65 after 30 min of incubation and return to normal level in 45 min (data not shown). ACP-I alone moderated the activation of p65 and its nuclear accumulation.

In addition, ACP-I inhibited LPS-induced degradation of IκBα (Figure 6C), thereby preventing the nuclear translocation of p65 (Figure 6B). These results suggested that ACP-I moderate NF-κB activation by restoring IκBα degradation in LPS-stimulated RAW 264.7 cells.

Effect of ACP-I on IL-8, IFN-β1, MIP-2, and RANTES expression in macrophages

Numerous immune cells, including phagocytes (neutrophils and macrophages), are involved in innate immune response, which is the first line of defense against infection and noxious stimuli (Marshall *et al.*, 2018). Macrophages

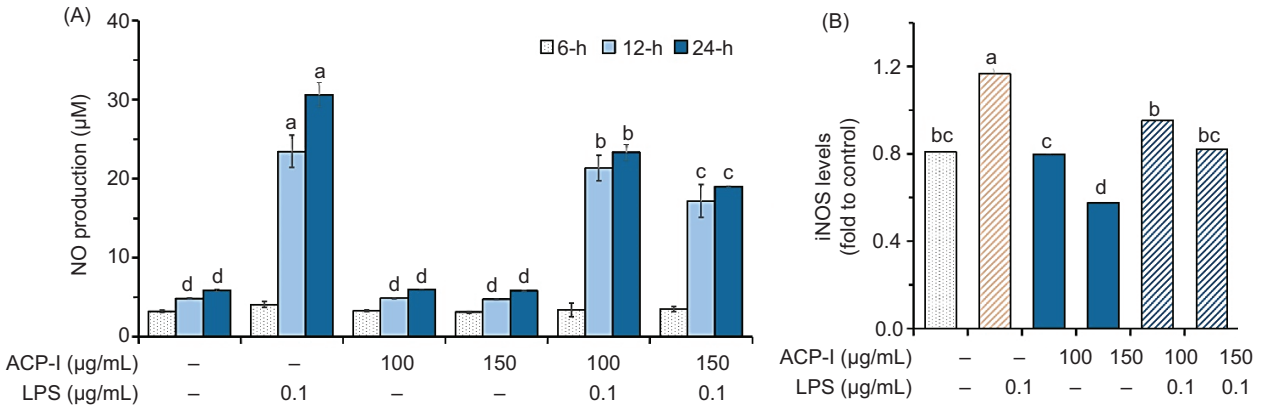

Figure 5. The anti-inflammatory activity of ACP-I in LPS-stimulated RAW 264.7 macrophages. (A) NO production after treatment for 6, 12, and 24 h; and (B) iNOS production after treatment for 24 h. Different letters indicate statistically significant differences ($P < 0.05$) vs. untreated cells.

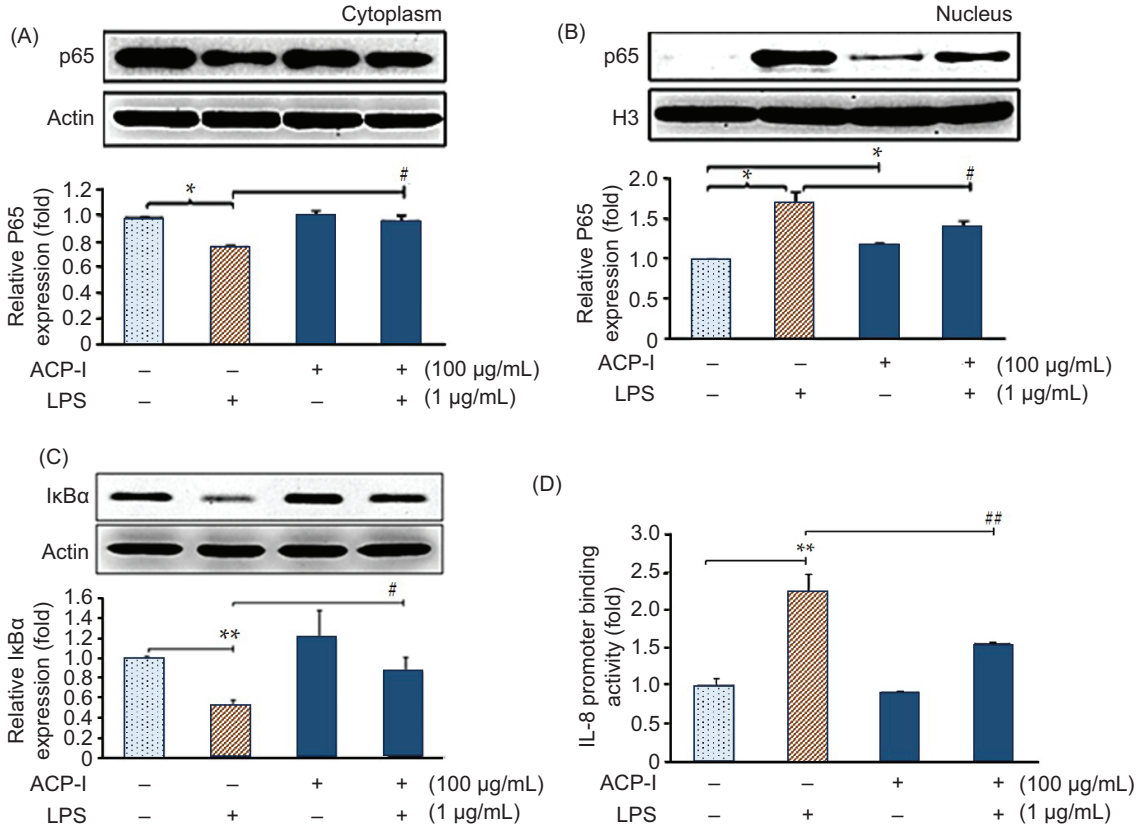

Figure 6. Effect of ACP-I on NF-κB activation in LPS-stimulated RAW 264.7 macrophages. Expression of (A) cytosolic NF-κB p65 subunit; (B) nuclear NF-κB p65 subunit; and (C) total NF-κB inhibitory protein (IκBα) after treatment with ACP-I for 24 h, followed by LPS for 30 min. (D) Expression of pro-inflammatory cytokine, IL-8 after treatment with ACP-I for 12 h, followed by LPS for 8 h. Statistical significance: *$P < 0.05$ and **$P < 0.01$ vs. untreated cells; #$P < 0.05$ vs. positive control, LPS-treated cells.

remove microorganisms and detoxify apoptotic cell debris by phagocytosis to control acute inflammatory response and regain homeostasis (Zhao *et al.*, 2021). Therefore, unsuccessful phagocytic clearance (e.g., prolonged pathogen exposure) can lead to septic shock and further progression of tissue damage and chronic inflammation (Zhao *et al.*, 2021). Macrophages induce NF-κB-dependent expressions of IL-8 to recruit granulocytes, primarily neutrophils, and macrophages *in situ* to drive upstream signaling events of pro-inflammatory response

at a site of damage or infection (Dorrington and Fraser, 2019). Simultaneously, IFN-β plays a key role in inhibiting IL-8 expression by binding to specific IL-8 promoters (Fan *et al.*, 2023; Zhao *et al.*, 2021). IFN-β is either low or not expressed in cells, and the activation, regulated by NF-κB, is a highly ordered process to avoid the harmful consequences of excessive inflammation (Dorrington and Fraser, 2019). Thus, IFN-β is considered a conserved key interface between innate and adaptive immunity (Fan *et al.*, 2023). However, the signaling pathways and regulatory factors of IFN-β are cell type-specific and not yet fully identified.

Herein, the expression of pro-inflammatory chemoattractants, including IL-8, IFN-β1, MIP-2 (for neutrophils), and RANTES (for granulocytes and lymphocytes), was measured in LPS-stimulated RAW 264.7 macrophages. Figure 6D shows the IL-8 promoter binding activity, observed by luciferase reporter assay indicating NF-κB p65-induced expression of IL-8 in RAW 264.7 cells. Considerably, ACP-I enhanced NF-κB activation (Figure 6C) without induction of IL-8 expression. In contrast with LPS alone, ACP-I modulated the activation of LPS-induced IL-8 promoter in RAW 264.7 cells. According to qRT-PCR data, IFN-β1, MIP-2, and RANTES production were upregulated in RAW 264.7 cells after treatment with ACP-I for 2–4 h (Figure 7A). ACP-I (100 μg/mL) modulated the expression of pro-inflammatory cytokines in a time-dependent manner. The cytokine expression increased significantly after 4 h for IFN-β1 (3.1-fold) and MIP-2 (2.5-fold) and after 2 h for RANTES (2.0-fold). No noticeable changes were found in morphology or cell death at all treatment time points (data not shown). Cytokine expression in response to ACP-I and LPS was shown in Figure 7B. LPS induced a noticeable increase in the production of IFN-β1 (6.7-fold) and RANTES (14.2-fold) in RAW 264.7 cells that, however, could be suppressed by pretreatment with ACP-I (100–150 μg/mL). In contrast, the production of MIP-2 was elevated in both ACP-I- and LPS-treated cells. Expression of MIP-2 messenger RNA (mRNA) increased by 2.3-fold after treatment with ACP-I (150 μg/mL) or LPS. A synergistic effect was observed if LPS-stimulated cells were pretreated with ACP-I at concentrations of 100 and 150 μg/mL (2.7- and 3.9-fold increase, respectively). The results indicated that ACP-I possessed

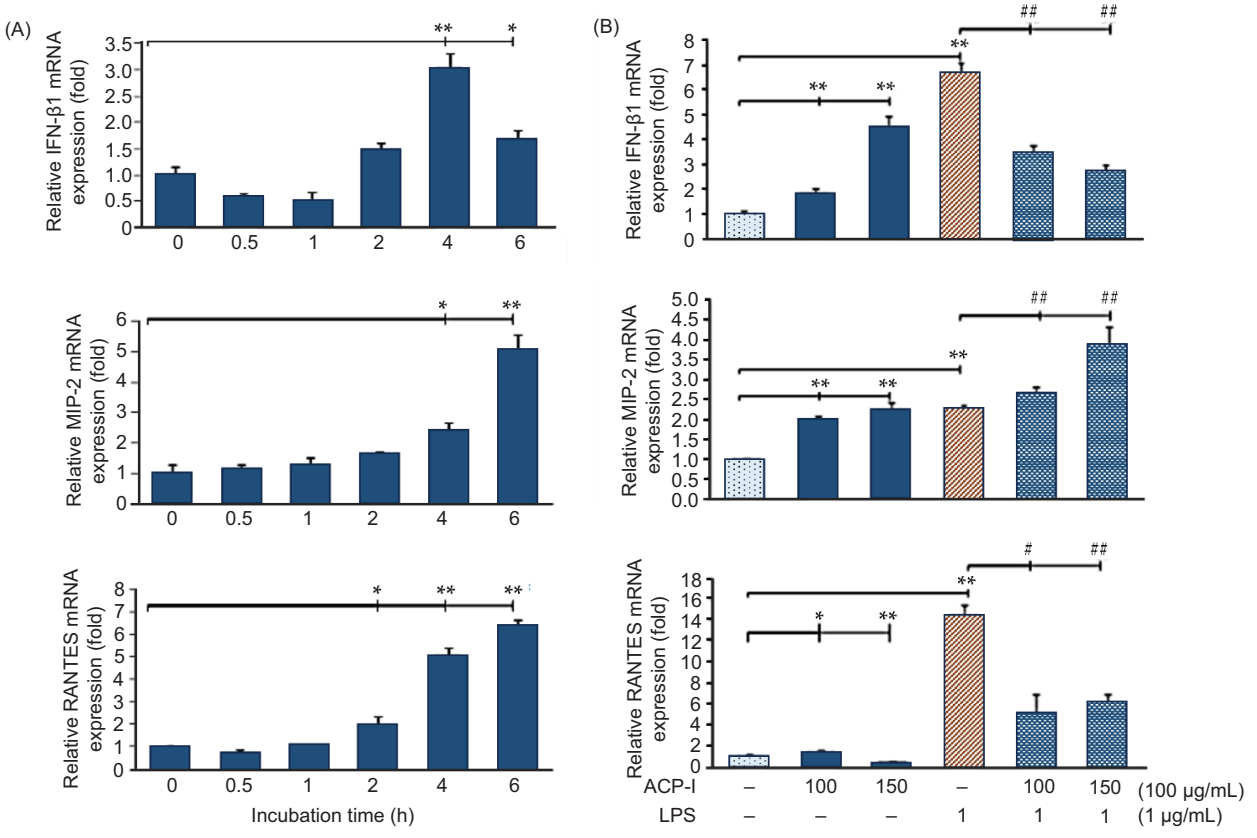

Figure 7. Expression of cytokines, IFN-β1, MIP-2, and RANTES in (A) RAW 264.7 macrophages after treatment with ACP-I (100 μg/mL) from 30 min to 6 h; and (B) LPS-stimulated RAW 264.7 macrophages after treatment with ACP-I for 24 h, followed by LPS for 4 h. Statistical significance: *$P < 0.05$ and **$P < 0.01$ vs. untreated cells; #$P < 0.05$ and ##$P < 0.01$ vs. positive control, LPS-treated cells.

immune-enhancing activity by suppressing the expression of IL-8, IFN-β1, and RANTES, but not MIP-2, in LPS-stimulated RAW 264.7 cells.

IL-8 is a potent activator and chemoattractant of neutrophils at sites of inflammation (Arango Duque and Descoteaux, 2014; Zhao *et al.*, 2021). The basal IL-8 is low in normal cells, but in inflamed cells, it is upregulated by the most abundantly activated monocytes and macrophages via NF-κB activation. Recently, excessive production of pro-inflammatory cytokines, such as IL-8 and IL-6, has been implicated as potential biomarkers for the diagnosis of inflammatory diseases, for example, acute ischemic stroke, severe coronavirus disease 2019, pathological pregnancies, and cancers (Kaur *et al.*, 2022).

Macrophages are likely to be the first cells to release IL-8 and are involved in acute inflammatory response (Arango Duque and Descoteaux, 2014). IFN-β is pivotal for downstream regulating macrophage function that alters the balance of pro-inflammatory cytokine levels regarding microbial characteristics, often referred to as PAMPs (Karimi *et al.*, 2020). IFN-β does not prevent the activation of NF-κB p65 but exerts an inhibitory effect on IL-8 expression. The present study revealed the impact of pretreatment with ACP-I (100 μg/mL) on suppression of NF-κB p65 nuclear translocation and expression of iNOS, IL-8, IFN-β1, and RANTES in LPS-stimulated RAW 264.7 cells, which suggested the immunomodulatory effects of ACP-I on pro-inflammatory cytokine expression and innate immunity.

Interestingly, ACP-I exerted dual functions to modulate chemokine C-X-C motif (CXC chemokines): IL-8 (CXCL8) and MIP-2 (CXCL2). Both chemokines are known as potent chemoattractants to recruit neutrophils at the site of infection. MIP-2 is mainly secreted by macrophages, also specialized macrophages, Kupffer cells in the liver. MIP-2 has a dual role of pro- and anti-inflammatory mediators that consequently impact the development of early immune responses and limit the progression of tissue injury (Qin *et al.*, 2017). Hence, an imbalance of the physiological level of MIP-2 results in a disorder between inflammation and tissue damage recovery.

This study's results indicated the anti-inflammatory activity of ACP-I via NF-κB signaling pathway. ACP-I (100 μg/mL) moderated the levels of IL-8 in RAW 264.7 macrophages after LPS challenge for 8 h (Figure 6D) by upregulating the corresponding inhibitor, IFN-β1, to reach maximum level at 4 h after the treatment and then a rapid decrease (Figure 7A). Meanwhile, MIP-2 level increased significantly after 4 h of LPS challenge, compared to untreated cells ($P < 0.05$), in accordance to RANTES, which mediates the trafficking and homing of T cells and monocytes (Zhao *et al.*, 2021). These findings implied that MIP-2 secretion involves multiple signaling pathways and T cell-mediated neutrophil recruitment. MIP-2 might be selectively upregulated to maintain immune response balance and prevent overactivation of neutrophils, which may lead to severe inflammation or tissue damage and propagation to septic shock (Zhang *et al.*, 2025). Thus, understanding the regulation of lymphocyte traffic during tolerance induction may lead to novel therapeutic approaches for antigen-specific immune response.

According to the results of the present study, ACP-I is a potential candidate for developing natural immune-modulating agents or adjuvants. It primarily involves the body's first line of defense against infection. During LPS stimulation, it moderates acute inflammatory response in macrophages within the first 30 min through preventing or restoring IκBα inhibitory proteins and consequently decreases levels of IFN-β1 and RANTES within 4 h. Meanwhile, it can act as a mitogen inducing MIP-2 levels to increase at 4 h and peak at 6 h post-LPS treatment. In-depth *in vitro* and *in vivo* evaluation of its therapeutic role and target through the TLR4-MAPK/NF-κB signaling pathway and upstream kinase inhibition should be explored to support potential clinical and industrial applications.

Overviewing the results

Brown rice, a whole grain and healthy diet, is consumed as a major staple food by nearly half of the global population. It consists of 7.1–8.3% protein, 1.6–2.8% fat, 73–76% digestible carbohydrates, 0.6–1.0% fiber, and 1.0–1.5% ash (Wu *et al.*, 2023). Despite its abundant nutritional and health benefits, BR is less accepted than polished and parboiled rice because of some barriers related to poor appearance, hard and chewy texture, short shelf life, and adverse effects, such as digestive disorders and anti-nutritional effects of phytate. Therefore, further research and development are needed to improve sensory attributes, shelf life, and bioactive components as well as increase the range of healthy food choices regarding BR.

Previous studies on SSF have used culinary-medicinal fungi to improve bioactive components and antioxidant activity of cereal grains and brans (Akbari *et al.*, 2023). During SSF of rice bran using *Pleurotus sapidus* for 10 days, total carbohydrates, protein, and ash increased by 13.6%, 5.4%, and 3.9%, respectively, whereas total fat decreased by 20.7% (Omarini *et al.*, 2019). The present study revealed change in MW of complex polysaccharide substrate after degradation into the fermented product (ACP-I) and fragments (ACP-II). ACP-I was identified to have immunomodulatory effects on

enhancing the proliferation of PBMCs while suppressing pro-inflammatory response in RAW 264.7 cells. Without clean-up process, the mitogenic activity of ACP-I is interfered with polysaccharide fragments and impurities, as observed in crude polysaccharide extract. In the authors' view, ACP-I was identified as a potential natural immunomodulator with both immune-stimulating and anti-inflammatory properties, distinguishing it from other fungal polysaccharides, such as β-glucans, which primarily exhibit immune-enhancing effects without significant anti-inflammatory activity. In addition, SSF was found to be a valuable process for the biomodification of BR's polysaccharides.

From a microbial aspect, AC can potentially enhance immunomodulatory functions of naturally occurring polysaccharides in BR with specific chemical modification during SSF. Further use of AC on the biomodification of polysaccharides in BR and plant-based industrial waste can develop an alternative bioprocess for bioactive polysaccharide production. SSF has shown advantageous competition with SmF for filamentous fungus cultivation, while more research is still needed to increase SSF capability for industrial process scale-up. From our knowledge, bench-scale production of AC is cost-efficient and provides uniform growth of AC mycelia. According to a previous report, fermentation duration has been optimized up to 10 months for the maximum bioactive polysaccharide production and their biological properties (Guo and Tseng, 2015). However, some disadvantages and research gaps in heat accumulation, growth kinetics, and container size or design of high-capacity packed-bed bioreactors must be overcome for rational design and process control in SSF.

Chemical structures of polysaccharides, especially MW, monosaccharides, and glycosidic linkages, are closely related to their biological functions. A previous study on 197 genotypes of rice (*O. sativa* L.) from 70 counties revealed composition of major monosaccharides, such as arabinose, xylose, mannose, galactose, fucose, and rhamnose, in whole grain (Panahabadi *et al.*, 2023). The fucose content is distributed in a high-density range of 12–24 μg/mg dry weight of whole grain, followed by arabinose (5–25 μg/mg), xylose (10–20 μg/mg), and galactose (2–8 μg/mg), except for mannose and rhamnose (<5 μg/mg).

In plants, α-(1→4)-D-galacturonan- and (1→6)-linked glucan enhance immune response. For edible fungi, β-(1→3)-D-glucan exerts immunomodulatory functions, while 1,6-linked glucan is likely associated with antioxidant activity and tumor immunology (Shen *et al.*, 2024). In addition to the linkages, branched and lower MW polysaccharides often show stronger immunomodulatory effects. Most studies on AC revealed classic linear (1→6)-D-galactans, which are substituted at the C-2 position either with L-fucose or 3-O-methylation of α-D-mannose and α-L-fucose residues (Li *et al.*, 2022). This study used AC in SSF to obtain bioactive polysaccharides under optimized conditions.

The 10-month-old fermented BR comprises a water-soluble bioactive polysaccharide, namely ACP-I, with a MW of 29.2 kDa. ACP-I is composed of galactose (43.75%), fucose (34.09%), and the minor content of glucose (14.20%), mannose (3.98%), and arabinose (3.98%). Structural analysis suggests that ACP-I consists of branched (1→3),(1→4)-α/β-D-galactan, and possibly (1→6)-α-D-galactan, substituted at O-2, O-3, and O-6 with 2,4-linked D-glucose, 2,4,6-linked L-arabinose, 3,4-linked D-galactose, and 1,6-linked D-galactose. The terminal α-L-fucose residues predominantly exist with a small amount of α-D-mannose and β-D-galactose. The inferred structural motif is consistent with the repeating unit of a branched heterogalactan with mixed (1→3),(1→4)-linkages and α-L-fucose and D-mannose terminals (Figure 8A). The side chains of (1→6)-α-D-galactose, substituted at C-2 with α-L-fucose, or α-D-mannose terminal, possibly exist (Figure 8B) according to previous studies on the water-soluble (1→6)-α-D-galactan and (1→6)-α-D-mannogalactan from AC mycelia that show α-L-fucose and α-D-mannose terminals (Cheng *et al.*, 2011; Liu *et al.*, 2017).

Given the scope of the present research, achieving precise and high-resolution structural data was not the primary objective. In addition, this study represents one of the first attempts to propose a speculative structure of ACP-I from Taiwanese *A. cinnamomea,* and the lack of information in the literature makes such speculation more challenging. Despite the above-mentioned limitations, the proposed structure is rational and supported by scientific evidence. At the same time, the current findings should be interpreted cautiously. Future research on detailed structural characterization and elucidation is needed to verify and refine the proposed preliminary model. In addition, a combination of structural characterization and *in vivo* study on the biological activities of ACP-I can provide valuable information on the structure–function relationship of this newly reported ACP-I.

Furthermore, chemical modification of AC polysaccharides to enhance anti-angiogenic activity has been reported, which can provide ideas for alternative structural and functional confirmatory research. For example, the sulfation modification of AC polysaccharides using the chlorosulfonic acid-pyridine method obtained a sulfated mannofucogalactan with a MW of 13.5 kDa. It was identified as a 1,6-linked galactose with branches substituted at O-2 of the 1,2,6-linked galactose residues in a molar ratio of approximately 3:1 with fucose (8.90%) and mannose (5.38%) terminals (Liu *et al.*, 2017).

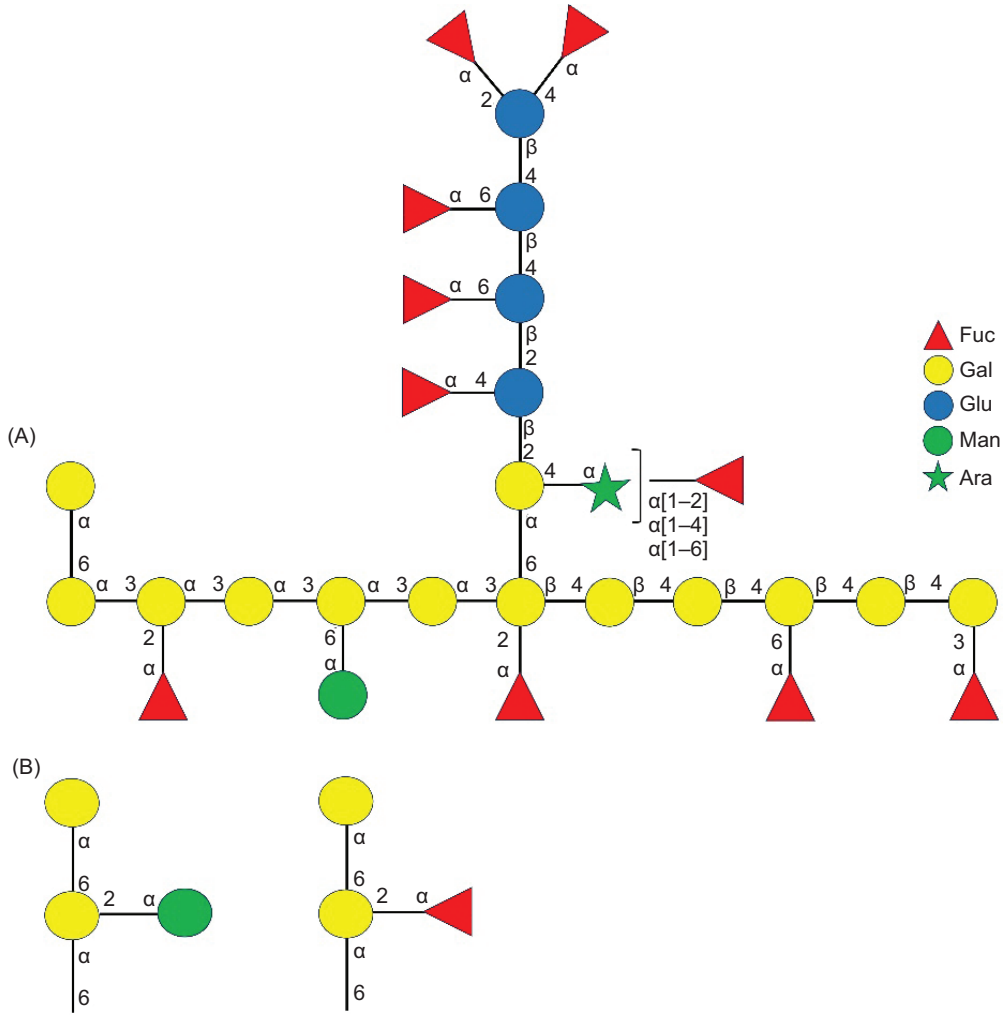

Figure 8. Schematic representation of the proposed chemical structure of ACP-I. Fuc: Fucose; Gal: Galactose; Glu: Glucose; Man: Mannose; Ara: Arabinose.

In addition, synthesis and biomanufacturing of glycosylation can modify protein-bound polysaccharides or glycoproteins. The 10-day-old fermented product of AC using SmF and potato dextrose broth primarily exists as a water-soluble fucosylated (1→6)-α-D-mannogalactan with partial 2,4-α-L-fucose terminals and a MW of 417 kDa (Cheng *et al.*, 2011). The major polysaccharide fraction contains galactose (42.73%) and fucose (11.97%), with the minor content of mannose (5.59%), sorbitol (3.47%), glucose (3.15%), fructose (2.27%), glucosamine (1.53%), and galactosamine (1.47%). A high MW antrodan (442 kDa), from SmF of AC mycelia has a complex structure of α- and β-glucans with (1→4) and (1→3)-linked glucose connecting to proteins that may be relevant to its potential in healing hepatotoxicity, non-alcoholic fatty liver, and lung cancer. However, it causes unpleasant responses in CD rats at a dosage exceeding 40 mg/kg body weight (Li *et al.*, 2022). Therefore, toxicity assessment and clinical development are the next steps, essentially for the large-scale synthesis and process scale-up of the polysaccharide production in the pharmaceutical and functional food industries.

PBMCs and RAW 264.7 models are used to screen putative immunomodulators. The present study indicated that ACP-I inhibited LPS-induced inflammation in RAW 264.7 cells by suppressing NF-κB activation and subsequent production of iNOS and pro-inflammatory cytokines, including IL-8, IFN-β1, and RANTES. Additionally, previous research has shown the coupled *in vitro* digestion method and Caco-2 human intestinal cell model to access intestinal inflammatory response to digested BR and parboiled germinated BR (Wu *et al.*, 2023). The pretreatment with their bioaccessible fractions attenuated the production of IL-8, monocyte chemoattractant protein-1 (MCP-1) and ROS in Caco-2

cells. However, the anti-inflammatory compounds were highlighted on their γ-aminobutyric acid (GABA) and phytochemical constituents.

Recently, the health benefits of BR have attracted more researchers to explore the relationship between BR diet and prevention of certain diseases. The chemical modification of fungal polysaccharides, particularly Basidiomycetes, is an alternative approach to obtain bioactive polysaccharides with immunomodulatory potential for functional food and pharmaceutical applications. In-depth explorations of the structure–function relationship are also required to unlock further their pharmaceutical and therapeutic benefits. Moreover, the therapeutic approach targeting NF-κB signaling has significant potential in treating acute inflammatory diseases and cancer. Thus, detailed elucidation of cell–cell communication among upstream signaling molecules involved in NF-kB activation can serve as potential pharmaceutical targets for anti-inflammatory and/or anti-carcinogenic effects.

Conclusions

A heteropolysaccharide, namely ACP-I, was isolated from the SSF of BR based on its immunomodulatory function. ACP-I had a MW of 29.2 kDa and predominant α- and β-D-galactose-linked backbone and side chains with terminal residues of L-fucose and a small amount of D-mannose and D-galactose. Pretreatment with ACP-I (100–150 μg/mL) could enhance the immune system and suppress LPS-induced inflammation in RAW 264.7 cells by downregulating the NF-κB activation and pro-inflammatory cytokine responses. ACP-I plays a crucial role as an immune modifier to enhance innate immunity and simultaneously suppress the stimulus-induced inflammation. Consequently, ACP-I has significant potential as a natural immunomodulator for functional foods and pharmaceuticals, particularly for enhancing innate immunity and managing chronic inflammation. The present study revealed a remarkable potential of ACP-I as a natural immunomodulator, targeting the NF-κB activation pathway to develop functional food additives and immunotherapy adjuvants. However, it is necessary to explore the structure–activity relationship as well as insight into the mechanism of the dual function of ACP-I, particularly in the regulation of CXC chemokines, including IL-8 and MIP-2, which have a significant impact on developing early immune responses and the outcome of tissue and liver injury. Their regulation mechanism *in vivo* and clinical trials remain to be elucidated for developing the chemokine-targeted immunotherapeutic strategies. Eventually, toxicity assessment and clinical development are crucial for the scale up of bioactive polysaccharide production in the functional food and pharmaceutical industries.

Data Availability Statement

Data are contained within the article as well as available upon request from the corresponding author.

Author Contributions

Potchanee Kaewkumsan, Wei-Ting Tseng, and Jia-Hsin Guo: conceptualization; Wei-Ting Tseng, and Jia-Hsin Guo: methodology; Wei-Ting Tseng: software and resources; Wei-Ting Tseng and Potchanee Kaewkumsan: validation; Potchanee Kaewkumsan and Wei-Ting Tseng: investigation; Potchanee Kaewkumsan: formal analysis, data curation, and writing—original draft preparation; Mohsen Gavahian and Jia-Hsin Guo: writing—review and editing; Wei-Ting Tseng and Potchanee Kaewkumsan: visualization; Jia-Hsin Guo and Mohsen Gavahian: supervision; Jia-Hsin Guo: project administration and funding acquisition. All authors had read and agreed to the published version of the manuscript.

Conflicts of Interest

The authors declared no conflict of interest.

Funding

This research was funded by the Pingtung Agricultural Biotechnology Park, Taiwan, grant No. 98AS-5.3.3-PT-f3(1).

References

Akbari, M., Razavi, S.H., Khodaiyan, F., Blesa, J. and Esteve, M.J. 2023. Fermented corn bran: a by-product with improved total phenolic content and antioxidant activity. Food Science and Technology (LWT) 184: 115090. https://doi.org/10.1016/j.lwt.2023.115090

Arango Duque, G. and Descoteaux, A. 2014. Macrophage cytokines: involvement in immunity and infectious diseases. Frontiers in Immunology 5: 491. https://doi.org/10.3389/fimmu.2014.00491

Bagaev, A.V., Garaeva, A.Y., Lebedeva, E.S., Pichugin, A.V., Ataullakhanov, R.I. and Ataullakhanov, F.I. 2019. Elevated pre-activation basal level of nuclear NF-κB in native macrophages accelerates LPS-induced translocation of cytosolic NF-κB into the cell nucleus. Scientific Reports 9: 4563. https://doi.org/10.1038/s41598-018-36052-5

Bai, L., Zhu, P., Wang, W. and Wang, M. 2020. The influence of extraction pH on the chemical compositions, macromolecular characteristics, and rheological properties of polysaccharide: the case of okra polysaccharide. Food Hydrocolloids 102: 105586. https://doi.org/10.1016/j.foodhyd.2019.105586

Barnes, W.J., Koj, S., Black, I.M., Archer-Hartmann, S.A., Azadi, P., Urbanowicz, B.R., Peña, M.J. and O'Neill, M.A. 2021. Protocols for isolating and characterizing polysaccharides from plant cell walls: a case study using rhamnogalacturonan-II. Biotechnology for Biofuels and Bioproducts 14: 142. https://doi.org/10.1186/s13068-021-01992-0

Bhanja, S.K. and Rout, D. 2017. Structural analysis of two bioactive components of an edible mushroom, *Termitomyces microcarpus*. Natural Product Communications 12: 1917–1920. https://doi.org/10.1177/1934578X1701201226

Black, I., Heiss, C. and Azadi, P. 2019. Comprehensive monosaccharide composition analysis of insoluble polysaccharides by permethylation to produce methyl alditol derivatives for gas chromatography/mass spectrometry. Analytical Chemistry 91: 13787–13793. https://doi.org/10.1021/acs.analchem.9b03239

Brown, G.D., Bauer, J., Osborn, H.M.I. and Kuemmerle, R. 2018. A solution NMR approach to determine the chemical structures of carbohydrates using the hydroxyl groups as starting points. ACS Omega 3: 17957–17975. https://doi.org/10.1021/acsomega.8b02136

Chaiwut, R. and Kasinrerk, W. 2022. Very low concentration of lipopolysaccharide can induce the production of various cytokines and chemokines in human primary monocytes. BMC Research Notes 15: 42. https://doi.org/10.1186/s13104-022-05941-4

Chakraborty, N., Banerjee, A., Sarkar, A., Ghosh, S. and Acharya, K. 2021. Mushroom polysaccharides: a potent immune-modulator. Biointerface Research in Applied Chemistry 11: 8915–8930. https://doi.org/10.33263/BRIAC112.89158930

Chen, D., Harris, P.J., Sims, I.M., Zujovic, Z. and Melton, L.D. 2017a. Polysaccharide compositions of collenchyma cell walls from celery (*Apium graveolens* L.) petioles. BMC Plant Biology 17: 104. https://doi.org/10.1186/s12870-017-1046-y

Chen, Q., Tang, H., Zha, Z., Yin, H., Wang, Y., Wang, Y., Li, H. and Yue, L. 2017b. β-D-glucan from *Antrodia camphorata* ameliorates LPS-induced inflammation and ROS production in human hepatocytes. International Journal of Biological Macromolecules 104: 768–777. https://doi.org/10.1016/j.ijbiomac.2017.05.191

Cheng, J.J., Lu, M.K., Lin, C.Y. and Chang, C.C. 2011. Characterization and functional elucidation of a fucosylated 1,6-α-d-mannogalactan polysaccharide from *Antrodia cinnamomea*. Carbohydrate Polymers 83(2): 545–553. https://doi.org/10.1016/j.carbpol.2010.08.016

Chylińska, M., Szymańska-Chargot, M. and Zdunek, A. 2016. FT-IR and FT-Raman characterization of non-cellulosic polysaccharides fractions isolated from plant cell wall. Carbohydrate Polymers 154: 48–54. https://doi.org/10.1016/j.carbpol.2016.07.121

Dong, Z., Liu, W., Zhou, D., Li, P., Wang, T., Sun, K., Zhao, Y., Wang, J., Wang, B. and Chen, Y. 2019. Bioactive exopolysaccharides reveal *Camellia oleifera* infected by the fungus *Exobasidium gracile* could have a functional use. Molecules 24: 2048. https://doi.org/10.3390/molecules24112048

Dorrington, M.G. and Fraser, I.D.C. 2019. NF-κB signaling in macrophages: dynamics, crosstalk, and signal integration. Frontiers in Immunology 10: 705. https://doi.org/10.3389/fimmu.2019.00705

Eltemur, D., Robatscher, P., Oberhuber, M., Scampicchio, M. and Ceccon, A. 2023. Applications of solution NMR spectroscopy in quality assessment and authentication of bovine milk. Foods 12: 3240. https://doi.org/10.3390/foods12173240

Emwas, A.H., Roy, R., McKay, R.T., Tenori, L., Saccenti, E., Gowda, G.A.N., Raftery, D., Alahmari, F., Jaremko, L., Jaremko, M. and Wishart, D.S. 2019. NMR spectroscopy for metabolomics research. Metabolites 9: 123. https://doi.org/10.3390/metabo9070123

Fan, J., Li, Q., Liang, J., Chen, Z., Chen, L., Lai, J. and Chen, Q. 2023. Regulation of IFNβ expression: focusing on the role of its promoter and transcription regulators. Frontiers in Microbiology 14: 1158777. https://doi.org/10.3389/fmicb.2023.1158777

Ganesan, N., Baskaran, R., Velmurugan, B.K. and Thanh, N.C. 2019. *Antrodia cinnamomea*—an updated mini review of its bioactive components and biological activity. Journal of Food Biochemistry 43: e12936. https://doi.org/10.1111/jfbc.12936

Glaros, V., Rauschmeier, R., Artemov, A.V., Reinhardt, A., Ols, S., Emmanouilidi, A., Gustafsson, C., You, Y., Mirabello, C., Björklund, Å.K., Perez, L., King, N.P., Månsson, R., Angeletti, D., Loré, K., Adameyko, I., Busslinger, M. and Kreslavsky, T. 2021. Limited access to antigen drives generation of early B cell memory while restraining the plasmablast response. Immunity 54: 2005–2023.e10. https://doi.org/10.1016/j.immuni.2021.08.017

Guo, J.H. and Tseng, W.T. 2015. Manufacturing Method for Obtaining Polysaccharide from the Solid-State Fermentation Product of *Antrodia cinnamomea*. Taiwan Patent TWI395813B. https://patents.google.com/patent/TWI395813B/en

Higashi, K. and Toida, T. 2017. Preparation of the partially methylated alditol acetates derived from CS tetrasaccharides containing galactose for the gas chromatography/mass spectrometry analysis. Bio-Protocol 7: e2600. https://doi.org/10.21769/BioProtoc.2600

Hou, C., Chen, L., Yang, L. and Ji, X. 2020. An insight into anti-inflammatory effects of natural polysaccharides. International Journal of Biological Macromolecules 153: 248–255. https://doi.org/10.1016/j.ijbiomac.2020.02.315

Ikeda, N., Yamaguchi, M. and Nishi, N. 2025. Health and economic impacts of increased brown rice consumption on type 2 diabetes in Japan: a simulation study, 2019–2029. Nutrients 17(3): 532. https://doi.org/10.3390/nu17030532

Jeon, R.L., Gilbert, C., Cheng, J., Putz, A.M., Dyck, M.K., Plastow, G.S., Fortin, F., Canada, P., Dekkers, J.C.M.andHarding, J.C.S. 2021. Proliferation of peripheral blood mononuclear cells from healthy piglets after mitogen stimulation as indicators of disease resilience. Journal of Animal Science 99: skab084. https://doi.org/10.1093/jas/skab084

Karimi, Y., Giles, E.C., Vahedi, F., Chew, M.V., Nham, T., Loukov, D., Lee, A.J., Bowdish, D.M. and Ashkar, A.A. 2020. IFN-β signalling regulates RAW 264.7 macrophage activation, cytokine production, and killing activity. Innate Immunity 26: 172–182. https://doi.org/10.1177/1753425919878839

Kleiveland, C.R. 2015. Peripheral blood mononuclear cells. In: Verhoeckx, K., Cotter, P., López-Expósito, I., Kleiveland, C., Lea, T., Mackie, A., Requena, T., Swiatecka, D., and Wichers, H. (eds.) The Impact of Food Bioactives on Health: *In vitro* and

Ex vivo Models. Springer International, AG Switzerland, pp. 161–167. https://doi.org/10.1007/978-3-319-16104-4

Li, H.X., Wang, J.J., Lu, C.L., Gao, Y.J., Gao, L. and Yang, Z.Q., 2022. Review of bioactivity, isolation, and identification of active compounds from *Antrodia cinnamomea*. Bioengineering 9(10): 494. https://doi.org/10.3390/bioengineering9100494

Liu, Y., Ding, Y., Ye, M., Zhu, T., Tian, D. and Ding, K. 2017. A novel heterogalactan from *Antrodia camphorata* and anti-angiogenic activity of its sulfated derivative. Polymers 9(6): 228. https://doi.org/10.3390/polym9060228

Manan, M.A. and Webb, C. 2017. Design aspects of solid state fermentation as applied to microbial bioprocessing. Journal of Applied biotechnology & Bioengineering 4(1): 511–532. https://doi.org/10.15406/jabb.2017.04.00094

Marshall, J.S., Warrington, R., Watson, W. and Kim, H.L. 2018. An introduction to immunology and immunopathology. Allergy, Asthma & Clinical Immunology 14(Suppl 2): 49. https://doi.org/10.1186/s13223-018-0278-1

Martynova, N.Y., Parshina, E.A. and Zaraisky, A.G. 2021. Protocol for separation of the nuclear and the cytoplasmic fractions of *Xenopus laevis* embryonic cells for studying protein shuttling. STAR Protocols 2: 100449. https://doi.org/10.1016/j.xpro.2021.100449

Mattedi, A., Sabbi, E., Farda, B., Djebaili, R., Mitra, D., Ercole, C., Cacchio, P., Del Gallo, M. and Pellegrini, M. 2023. Solid-state fermentation: applications and future perspectives for biostimulant and biopesticides production. Microorganisms 11: 1408. https://doi.org/10.3390/microorganisms11061408

Molelekoa, T.B.J., Regnier, T., da Silva, L.S. and Augustyn, W. 2021. Production of pigments by filamentous fungi cultured on agro-industrial by-products using submerged and solid-state fermentation methods. Fermentation 7: 295. https://doi.org/10.3390/fermentation7040295

Nepravishta, R., Monaco, S., Distefano, M., Rizzo, R., Cescutti, P. and Angulo, J. 2021. Multifrequency STD NMR unveils the interactions of antibiotics with *Burkholderia multivorans* biofilm exopolysaccharide. Frontiers in Molecular Biosciences 8: 727980. https://doi.org/10.3389/fmolb.2021.727980

Omarini, A.B. Labuckas, D. Zunino, M.P., Pizzolitto, R., Fernández-Lahore, M., Barrionuevo, D. and Zygadlo, J.A. 2019. Upgrading the nutritional value of rice bran by solid-state fermentation with *Pleurotus sapidus*. Fermentation 5: 44. https://doi.org/10.3390/fermentation5020044

Palmieri, E.M., McGinity, C., Wink, D.A. and McVicar, D.W. 2020. Nitric oxide in macrophage immunometabolism: hiding in plain sight. Metabolites 10: 429. https://doi.org/10.3390/metabo10110429

Panahabadi, R., Ahmadikhah, A. and Farrokhi, N. 2023. Genetic dissection of monosaccharides contents in rice whole grain using genome-wide association study. Plant Genome 16(4): e20292. https://doi.org/10.1002/tpg2.20292

Peakman, M., Tredger, J.M., Davies, E.T., Davenport, M., Dunne, J.B., Williams, R. and Vergani, D. 1993. Analysis of peripheral blood mononuclear cells in rodents by three-colour flow cytometry using a small-volume lysed whole blood technique. Journal of Immunological Methods 158: 87–94. https://doi.org/10.1016/0022-1759(93)90261-5

Pérez-Bassart, Z., Bäuerl, C., Fabra, M.J., Martínez-Abad, A., Collado, M.C. and López-Rubio, A. 2023. Composition, structural properties and immunomodulatory activity of several aqueous *Pleurotus* β-glucan-rich extracts. International Journal of Biological Macromolecules 253(6): 127255. https://doi.org/10.1016/j.ijbiomac.2023.127255

Poškaitė, G., Wheatley, D.E., Wells, N., Linclau, B. and Sinnaeve, D. 2023. Obtaining pure ^{1}H NMR spectra of individual pyranose and furanose anomers of reducing deoxyfluorinated sugars. Journal of Organic Chemistry 88: 13908–13925. https://doi.org/10.1021/acs.joc.3c01503

Punthi, F., Mulyani, R., Chang, C.K., Adi, P., Gavahian, M., Yudhistira, B., Listyaningrum, R.S., Cheng, K.C., Hou, C.Y. and Hsieh, C.W. 2025. Enhanced extraction of *Pleurotus ostreatus* polysaccharides via plasma-ultrasound synergy: kinetics modeling and functional characterization. Innovative Food Science & Emerging Technologies 103: 104046. https://doi.org/10.1016/j.ifset.2025.104046

Punthi, F., Yudhistira, B., Gavahian, M., Chang, C.K., Husnayain, N., Hou, C.Y., You, C.C. and Hsieh, C.W. 2023. Optimization of plasma activated water extraction of *Pleurotus ostreatus* polysaccharides on its physiochemical and biological activity using response surface methodology. Foods 12(23): 4347. https://doi.org/10.3390/foods12234347

Qin, C.C., Liu, Y.N., Hu, Y., Yang, Y. and Chen, Z. 2017. Macrophage inflammatory protein-2 as mediator of inflammation in acute liver injury. World Journal of Gastroenterology 23(17): 3043–3052. https://doi.org/10.3748/wjg.v23.i17.3043

Režić-Mužinić, N., Mastelić, A., Benzon, B., Markotić, A., Mudnić, I., Grković, I., Grga, M., Milat, A.M., Ključević, N. and Boban, M. 2018. Expression of adhesion molecules on granulocytes and monocytes following myocardial infarction in rats drinking white wine. PLoS ONE 13: e0196842. https://doi.org/10.1371/journal.pone.0196842

Sankar, M., Mathew, R.M., Puthiyamadam, A., Sreeja-Raju, A., Christopher, M., Gokhale, D.V. and Sukumaran, R.K. 2023. Comparison of the solid-state and submerged fermentation derived secretomes of hyper-cellulolytic *Penicillium janthinellum* NCIM 1366 reveals the changes responsible for differences in hydrolytic performance. Bioresource Technology 371: 128602. https://doi.org/10.1016/j.biortech.2023.128602

Shen, Y., Zhao, H., Wang, X., Wu, S., Wang, Y., Wang, C., Zhang, Y. and Zhao, H. 2024. Unraveling the web of defense: the crucial role of polysaccharides in immunity. Frontiers in Immunology 15: 1406213. https://doi.org/10.3389/fimmu.2024.1406213

Speciale, I., Notaro, A., Garcia-Vello, P., Di Lorenzo, F., Armiento, S., Molinaro, A., Marchetti, R., Silipo, A. and De Castro, C. 2022. Liquid-state NMR spectroscopy for complex carbohydrate structural analysis: a hitchhiker's guide. Carbohydrate Polymers 277: 118885. https://doi.org/10.1016/j.carbpol.2021.118885

Tucureanu, M.M., Rebleanu, D., Constantinescu, C.A., Deleanu, M., Voicu, G., Butoi, E., Calin, M. and Manduteanu, I. 2018. Lipopolysaccharide-induced inflammation in monocytes/

macrophages is blocked by liposomal delivery of Gi-protein inhibitor. International Journal of Nanomedicine 13: 63–76. https://doi.org/10.2147/IJN.S150918

Vargas-Maya, N.I., Padilla-Vaca, F., Romero-González, O.E., Rosales-Castillo, E.A.S., Rangel-Serrano, Á., Arias-Negrete, S. and Franco, B. 2021. Refinement of the Griess method for measuring nitrite in biological samples. Journal of Microbiological Methods 187: 106260. https://doi.org/10.1016/j.mimet.2021.106260

Vetvicka, V., Teplyakova, T.V., Shintyapina, A.B. and Korolenko, T.A. 2021. Effects of medicinal fungi-derived β-glucan on tumor progression. Journal of Fungi (Basel) 7: 250. https://doi.org/10.3390/jof7040250

Wang, C., Zhang, W., Wong, J.H., Ng, T. and Ye, X. 2019. Diversity of potentially exploitable pharmacological activities of the highly prized edible medicinal fungus *Antrodia camphorata*. Applied Microbiology and Biotechnology 103: 7843–7867. https://doi.org/10.1007/s00253-019-10016-9

Wu, X., Guo, T., Luo, F. and Lin, Q. 2023. Brown rice: a missing nutrient-rich health food. Food Science and Human Wellness 12: 1458–1470. https://doi.org/10.1016/j.fshw.2023.02.010

Wu, M.L., Shen, T.L., Chang, T.T., Chang, C.H., Hung, T.H., Lee, C.Y. and Lin, C.Y. 2015. Establishment of a rapid PCR detection method for *Antrodia salmonea* and *A. cinnamomea*. Taiwan Journal of Forest Science 30(1): 45–53. https://doi.org/10.7075/TJFS.201503_30(1).0004

Xia, Y., Meng, P., Liu, S., Tan, Z., Yang, X., Liang, L., Xie, F., Zhang, H., Wang, G., Xiong, Z., Lo, J. and Ai, L. 2022. Structural and potential functional properties of alkali-extracted dietary fiber from *Antrodia camphorata*. Frontiers in Microbiology 13: 921164. https://doi.org/10.3389/fmicb.2022.921164

Yue, G.G., Chan, B.C., Hon, P.M., Kennelly, E.J., Yeung, S.K., Cassileth, B.R., Fung, K.P., Leung, P.C. and Lau, C.B. 2010. Immunostimulatory activities of polysaccharide extract isolated from *Curcuma longa*. International Journal of Biological Macromolecules 47: 342–347. https://doi.org/10.1016/j.ijbiomac.2010.05.019

Yue, F., Zhang, J., Xu, J., Niu, T., Lü, X. and Liu, M. 2022. Effects of monosaccharide composition on quantitative analysis of total sugar content by phenol-sulfuric acid method. Frontiers in Nutrition 9: 963318. https://doi.org/10.3389/fnut.2022.963318

Zhang, B.B., Guan, Y.Y., Hu, P.F., Chen, L., Xu, G.R., Liu, L. and Cheung, P.C.K. 2019. Production of bioactive metabolites by submerged fermentation of the medicinal mushroom *Antrodia cinnamomea*: recent advances and future development. Critical Reviews in Biotechnology 39: 541–554. https://doi.org/10.1080/07388551.2019.1577798

Zhang, J., Shao, Y., Wu, J., Zhang, J., Xiong, X., Mao, J., Wei, Y., Miao, C. and Zhang, H. 2025. Dysregulation of neutrophil in sepsis: recent insights and advances. Cell Communication and Signaling 23: 87. https://doi.org/10.1186/s12964-025-02098-y

Zhao, H., Wu, L., Yan, G., Chen, Y., Zhou, M., Wu, Y. and Li, Y. 2021. Inflammation and tumor progression: signaling pathways and targeted intervention. Signal Transduction and Targeted Therapy 6: 263. https://doi.org/10.1038/s41392-021-00658-5

Supplementary

Table S1. Cell cytotoxicity assay on rat PBMC and RAW 264.7 mouse macrophage cells.

Treatment	Cell viability (fold to control)								
	PBS	LPS		Con A	ACP-I				
Final concentration (μg/mL)		0.1	1	10	50	100	150	200	250
Rat PBMC cells[a]	–	–	1.49 ± 0.08*	1.90 ± 0.11*	–	–	6.08 ± 0.14*	-	–
RAW 264.7 mouse macrophage cells[b]	0.97 ± 0.04	0.90 ± 0.02*	0.92 ± 0.02*	–	0.95 ± 0.01	0.94 ± 0.02	0.95 ± 0.02	0.94 ± 0.01	0.95 ± 0.01

Notes: [a]The cells were treated with RPMI-1640 medium for 72 h.
[b]The cells were treated in RPMI-1640 medium, supplemented with 10% FBS and 1% penicillin–streptomycin for 24 h.
The data are presented as mean ± SD; *significant difference ($P < 0.05$) compared to the control group.